Diploma Thesis

Effect of field-inhomogeneity corrections on functional MRI based activity maps

Milán Márton Tüske

Supervisor: Gyula Gyebnár, PhD.
Physicist
Semmelweis University Medical Imaging Centre
Department of Neuroradiology

Consultant: Ferenc Simon
Professor
Budapest University of Technology and Economics
Department of Physics

Budapest University of Technology and Economics
2026

Szakdolgozat-választás

A hallgató neve: Tüske Milán	specializációja: Orvosi fizika MSc
A záróvizsgát szervező tanszék neve: Fizika Tsz.	

A témavezető neve: Dr. Gyebnár Gyula - munkahelye: Semmelweis Egyetem, Neuroradiológia Tanszék - beosztása: tudományos munkatárs, MR fizikus - email címe: gyebnar.gyula@semmelweis.hu	A konzulens neve: Dr. Simon Ferenc - tanszéke: Fizika Tsz. - beosztása: Egyetemi tanár - email címe: simon.ferenc@ttk.bme.hu

A kidolgozandó feladat címe: Térinhomogenitás-korrekciók hatása funkcionális MRI felvételekből számolt aktivitástérképeken

A téma rövid leírása, a megoldandó legfontosabb feladatok felsorolása:

A funkcionális MRI (fMRI) felvételeket alap- és klinikai kutatásokban elterjedten alkalmazzák,[1] idegsebészeti beavatkozások tervezése során a védendő, különböző funkciókat egészségesen ellátó agyterületek egyedi aktivitási mintázatának meghatározásában kapnak szerepet. [2] A neuronális aktivitás lokális fokozódására a területre áramló vér oxigenizáltságának megfigyelésén (blood-oxygen level dependent, BOLD) keresztül következtethetünk. Feladatfüggő fMRI vizsgálatokban az aktivációs térképek meghatározásának alapja a BOLD-jel fluktuációinak időbeli korrelációja a feladatot leíró paradigmával. A felvételek értékelésében fontos a megfelelő statisztikai erő, melynek alapját a részletes térbeli és időbeli felbontás, valamint a jó képminőség adja. [3,4]

A Semmelweis Egyetem Orvosi Képalkotó Klinika részeként működő Neuroradiológia Tanszék Philips Ingenia 3T MRI berendezésén rutinszerűen végzünk preoperatív feladatfüggő fMRI vizsgálatokat. A felvételek készítéséhez használt gradiens-echo EPI (GRE-EPI) szekvencia az évek során több változáson esett át a térbeli és időbeli felbontás növelése érdekében (pl. szimultán többszeletes képalkotás alkalmazásával). A tervezett kutatási projektben olyan posztrekonstrukciós korrekciós eljárások alkalmazását vizsgálnánk, melyekkel a mágneses tér lokális inhomogenitásából, valamint egyéb intenzitásingadozásokból eredő képtorzulások mértéke potenciálisan csökkenthető, ezzel a vizsgálatok statisztikai ereje, így diagnosztikai hasznossága is javítható.

A hallgató feladatai:

- Az fMRI mérés és adatfeldolgozás módszertani alapjainak, a jellemző műtermékeknek, valamint ezek kezelési eljárásainak megismerése, irodalomkutatás.
- A Tanszéken korábban gyűjtött felvételeknél alkalmazott eljárások és feldolgozó szoftverek megismerése.
- Részvétel további feladatfüggő fMRI adatok gyűjtésében.
- A gyűjtött adatok feldolgozása, korrekciós eljárások alkalmazása, a korrekció aktivációs térképekre gyakorolt hatásának értékelése.

Referenciák:

1. Orringer, D.A., D.R. Vago, and A.J. Golby, *Clinical applications and future directions of functional MRI.* Semin Neurol, 2012. **32**(4): p. 466-75.
2. Haller, S. and A.J. Bartsch, *Pitfalls in FMRI.* Eur Radiol, 2009. **19**(11): p. 2689-706.
3. Kozák, L.R., et al., *[Functional magnetic resonance imaging for cortical mapping in epilepsy].* Ideggyogy Sz, 2011. **64**(9-10): p. 294-9.
4. Poldrack, Russell A. et al. “Handbook of Functional MRI Data Analysis: Index.” (2011).

A záróvizsga kijelölt tételei:

Dátum:

Hallgató aláírása:	Témavezető aláírása*:	Tanszéki konzulens aláírása:	A témakiírását jóváhagyom (tanszékvezető aláírása):

*A témavezető jelen feladatkiírás aláírásával tudomásul veszi, hogy a BME TVSZ 145. és 146.§ alapján az egyetem a képzési célok megvalósulása érdekében a szakdolgozatok, illetve diplomamunkák nyilvánosságát tartja elsődlegesnek. A hozzáférés korlátozása csak kivételes esetben, a dékán előzetes hozzájárulásával lehetséges.

Declaration of originality

Undersigned Milán Márton Tüske, medical physics MSc student of the Budapest University of Technology and Economics, declare that I wrote this thesis without the use of any unauthorized assistance, under the guidance of my supervisor. I have cited every source I used. For any part that I have borrowed verbatim, or paraphrased while preserving its original meaning, I have marked its source of origin.

Budapest, 2026. 05. 29.

_____

Milán Márton Tüske

Identicality of digital and printed versions

Undersigned Milán Márton Tüske medical physics MSc student of the Budapest University of Technology and Economics, declare that the digital and printed copies of the thesis are identical in all respects.

Budapest, 2026. 05. 29.

Milán Márton Tüske

Acknowledgements

I would like to express my gratitude to my supervisors, Noémi Gyüre and Dr. Gyula Gyebnár. This thesis would not have been possible without their guidance and assistance. I would also like to thank Dr. Lajos Rudolf Kozák for his insights on the results. I would also like to thank my consultant, Dr. Ferenc Simon, for his helpful feedback on this thesis.

I would also like to thank all my friends who participated as volunteers in the measurements.

Last but not least, I would like to thank my family and friends for all the encouragement and support they have given me over the years.

This work was supported by the National Research, Development and Innovation Office of Hungary (NKFIH) Grant Nr. 149457.

Contents

List of abbreviations

BOLD	Blood oxygen level dependent
DEPM	Dual-echo phase mapping
ETL	Echo train length
EES	Effective echo spacing
fMRI	Functional magnetic resonance imaging
FWER	Family-wise error rate
FWHM	Full width at half maximum
GLM	General Linear Model
GRE-EPI	Gradient-echo echo planar imaging
HARDI	High Angular Resolution Diffusion Imaging
IF	Imaging frequency
MNI	Montreal Neurological Institute
NMI	Normalised mutual information
OPED	Opposing phase encoding directions
PE	Phase-encoding
PRF	Parallel reduction factor
ROI	Region of interest
SE-EPI	Spin-echo echo planar imaging
SNR	Signal-to-noise ratio
VDM	Voxel displacement map
WFS	Water-fat shift

Chapter 1

Introduction

The human brain is a complex organ whose functionality is still researched to this day. The continuously improving medical imaging methods make it possible to deepen the knowledge about the brain's functionality. This is especially important for understanding cognitive processes and neurological disorders in depth.

Functional magnetic resonance imaging (fMRI) examinations are widely used both in basic and clinical research[1]. Local increases of neural activity in the brain can be inferred by measuring the oxygenation of the area's perfusion (blood-oxygen level dependent signal, BOLD). In task-based fMRI studies, activation maps are calculated based on the temporal correlation of fluctuations in the BOLD signal and the timings of the task-specific paradigm[2].

At the Department of Neuroradiology of the Semmelweis University Medical Imaging Centre, preoperative task-based fMRI scans are routinely acquired on a Philips Ingenia 3T MRI scanner. The gradient-echo echo planar imaging (GRE-EPI) sequence used for image acquisition has undergone several changes over the years in order to increase temporal and spatial resolution and thereby improve the reliability of the results.

In the present work, multiple task-based fMRI scans of healthy young volunteers were analysed. We investigated several post-reconstruction correction methods to reduce image distortion and intensity fluctuations resulting from local inhomogeneities of the B_0 magnetic field. Our aim was to refine image quality, thus improving the reliability and clinical utility of the results.

We selected various task-based fMRI paradigms to examine how the inhomogeneity correction affects the different activation maps.

In this thesis, I summarise the basics of fMRI and the applied B_0 inhomogeneity correction methods. I also cover the acquisition method, the data processing pipeline, the calculation of activation maps, and the extent to which the B_0 inhomogeneity correction affects the obtained results.

Chapter 2

Theoretical background

2.1 Functional MRI

In functional MRI, local brain activity can be inferred from changes in blood perfusion of the area. Brain activity requires energy, which is covered by breaking the high-energy bond of adenosine triphosphate (ATP), and ATP synthesis requires glucose and oxygen. Oxygen is transported to the brain cells by hemoglobin in red blood cells. Locally increasing brain activity requires more oxygen, resulting in increased perfusion. At first, the concentration of deoxyhemoglobin rises, but soon the increased perfusion results in a few percent increase in the ratio of oxygenated and deoxygenated hemoglobin concentrations. This will affect the local T_2^* relaxation time, because deoxyhemoglobin is slightly paramagnetic, while most tissues and oxygenated hemoglobin are diamagnetic. This is the background of functional MRI based on the Blood Oxygen Level Dependent(BOLD) contrast. In order for the BOLD signal to be adequately sampled across the entire brain, the MRI scan must be performed with a measurement sequence that results in sufficiently fine temporal and spatial resolution. The sequence most commonly used for BOLD-fMRI is the gradient-echo echo planar imaging (GRE-EPI). The sequence diagram for the GRE-EPI can be seen on Figure 2.1. Using EPI sequences, a single excitation is enough to sample the whole k-space for a slice. Fourier transform is used to reconstruct images from k-space data.

Task-based fMRI

In task-based fMRI, different task-specific paradigms are used depending on which brain region needs to be examined. During the paradigm, a series of GRE-EPI images are acquired with a typical temporal resolution of 1-3 seconds and a spatial resolution of 2-3 mm isotropic voxels. The positive BOLD-signal's timing will correlate with the timing of the paradigm's task. The most widely used way to calculate activation maps is with General Linear Models (GLM).

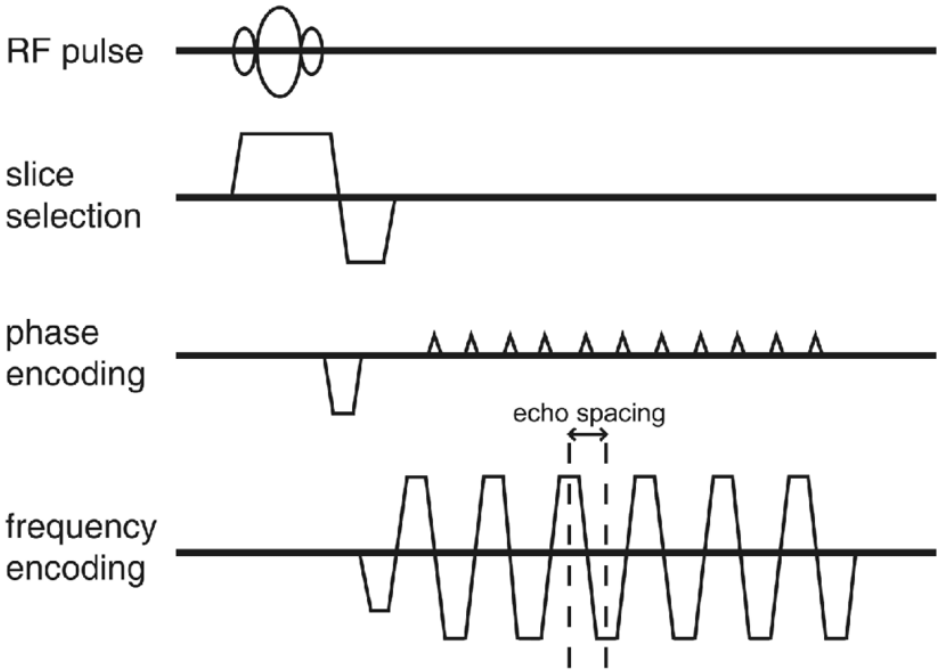

Figure 2.1: The sequence diagram of GRE-EPI[3]

2.2 Effect of field inhomogeneities

During image acquisition, the B_0 field is not entirely homogeneous, even after shimming. Additionally, when a subject is in the scanner, the magnetisation of their body also affects the magnetic field. This inhomogeneity causes phase-shifts in our signal, and causes voxels to shift along the phase-encoding direction [4]. The amount of phase-shift can be given by

$$\Delta\phi = \gamma \Delta B_0(x,y,z)t, \tag{2.1}$$

where $\gamma = 42.58$ MHz/T is the gyromagnetic ratio for Hydrogen-1, $\Delta B_0(x,y,z)$ is the deviation from B_0, and t is the elapsed time. Under typical conditions, if $B_0 = 3$ Tesla, the readout time for a GRE-EPI slice with 3 mm isotropic resolution is 0.04 s, and the inhomogeneity is $\frac{\Delta B_0}{B_0} = 1$ ppm, the resulting shift will be 5 voxels, or 15 mm.

2.3 Preprocessing

In order to improve signal-to-noise ratio (SNR)[1] and mitigate unwanted artefacts, raw fMRI images need multiple preprocessing steps before calculating activation maps. Slight movement during image acquisition, even due to breathing or swallowing, impacts image quality, as well as the acquisition protocol. There are many different preprocessing steps[2], in the following paragraphs, I briefly describe those that we used.

Realignment and unwarping

Movement during image acquisition is one of the biggest problems in fMRI. One way to correct this is by realigning all volumes to a reference volume (usually the first volume) with rigid body transformations. During this step, a calculated Voxel Displacement Map (VDM) can also be applied to correct for the displacement caused by B_0 field inhomogeneities with a non-linear transformation.

Slice timing correction

In fMRI, it is important to sample the BOLD signal as frequently as possible. Because of 2-dimensional imaging, the slices in our volume will be acquired one after the other, with a time difference between each slice. With slice timing correction, a reference slice can be selected, and every other slice's signal can be processed in relation to the reference slice's timing.

Segmentation

Segmentation allows us to separate the studied volume based on its main tissue properties. In our case, the main tissue types within the bony skull are cerebrospinal fluid, grey matter, and white matter.

Coregistering functional and anatomical images

During the evaluation of the results, we use images with different contrasts (e.g., T_1-weighted images for anatomical localisation). Since not all images are acquired in the

[1]Functional SNR is the ratio between the active-passive BOLD amplitude differences and the signal variability through the blocks of the paradigm.

same coordinate system, coregistration is needed to align them. Coregistration happens by maximising the Normalised Mutual Information (NMI) calculated by

$$\mathrm{NMI}(A,B) = \frac{H(A) + H(B)}{H(A,B)}, \tag{2.2}$$

where

$$H(X) = \sum_i p(x_i) \log_2(x_i), \tag{2.3}$$

where p is the probability of a given voxel, calculated from a binned histogram of x_i values[5]. A higher NMI value represents a better fit between the two images.

Normalisation

Every brain is unique, normalisation means transforming our subjects' coordinates into a standardised coordinate system. This is especially important when aiming to perform group-level analyses. With group-level analyses, we can calculate statistics, compare different groups, paradigms, and preprocessing methods. The most commonly used standardised brain template is Montreal Neurological Institute-152 (MNI-152)[6].

Smoothing

During spatial smoothing, fMRI data is convolved with a Gaussian kernel, with a chosen full width at half maximum (FWHM). The aim of this step is to filter out high spatial frequency noise and to improve the functional signal-to-noise ratio as well.

2.4 Inhomogeneity correction

Before realignment and unwarping of the functional data, several correction methods can be used to counteract image distortions caused by field inhomogeneities. Most of these methods require the acquisition of a field map. Several strategies have been proposed to measure field maps, but here we mention only those that we used.

Dual-echo Phase Mapping (DEPM)

One correction method involves acquiring two gradient-echo images of the whole brain with different echo times, and calculating a field map[7]. To calculate the field map, the equation

$$\Delta B_0(x,y,z) = \frac{1}{2\pi\gamma\Delta TE}\Delta\phi(x,y,z) \tag{2.4}$$

is used, where ΔB_0 is the inhomogeneity in Tesla, ΔTE is the difference between the two echo times, $\Delta\phi$ is the phase difference between the two images, and γ is the gyromagnetic ratio.

Phase unwrapping

As the MRI signal is measured as complex values, the magnitude and phase information of the images can be reconstructed separately. The magnitude image contains the intensity of the voxels, and the phase image contains the phase of the voxels between π and $-\pi$. Due to this limited $[-\pi, \pi]$ range, the phase values wrap around at the boundaries, causing sharp jumps on these images - commonly referred to as 'wraps'. An example pair of images can be seen on Figure 2.2.

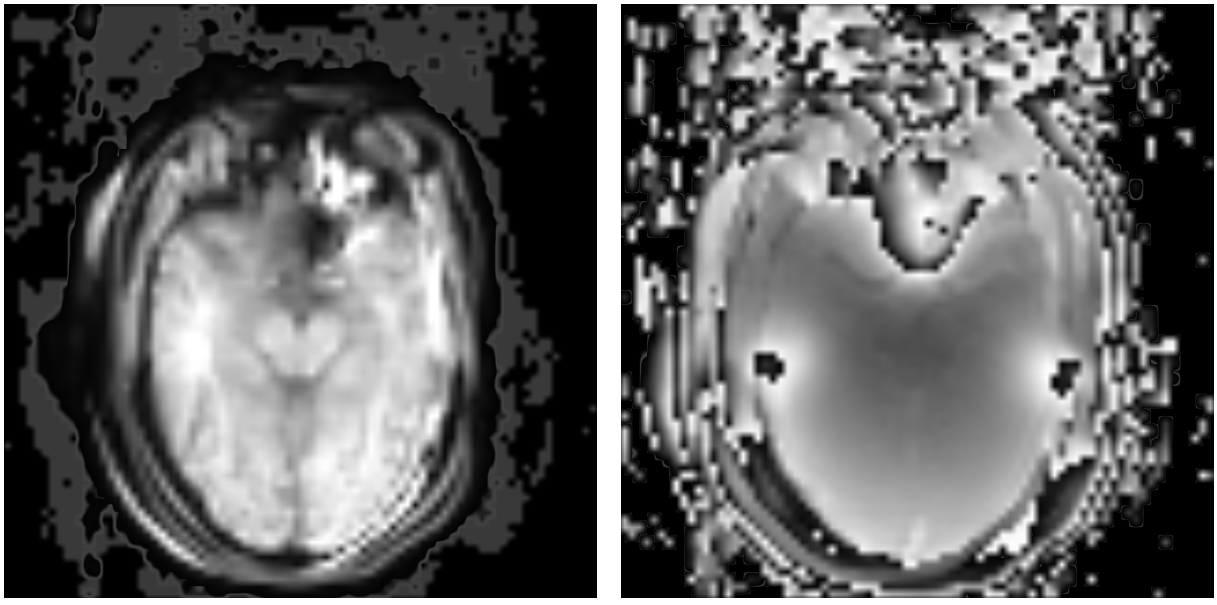

(a) (b)

Figure 2.2: An example magnitude (a) and phase (b) image from an acquired GRE acquisition. On the phase image, a wrap occurs when the bright regions sharply change to black.

There are different methods that attempt to unwrap the phase jumps in the images, but here we only mention the main steps of the one that is implemented in SPM and we use[8].

The first step of the unwrapping is to divide the whole brain into N regions. The initial regions are chosen by splitting up the volume into connected components, inside which no phase wrapping happens. This is done by partitioning the range of phase values into N regions. For example, if $N = 3$, the initial partitions are $\{[-\pi,-\pi/3),[-\pi/3,\pi/3),[\pi/3,\pi)\}$. After constructing the initial regions, a cost function is defined that penalises phase-differences along interfacing regions. Then an algorithm merges two selected regions along an interface where the cost is the largest, and minimizing the overall cost after the merge. Consequently, two new regions are selected to be merged, and the algorithm repeats until no more interfaces remain between regions, thus creating one large region without wraps.

Opposing Phase Encoding Directions (OPED)

Another way to correct geometric distortions is to acquire two spin-echo echo planar imaging (SE-EPI) images with opposite phase-encoding (PE) directions[2][9]. This will cause the voxel displacements to have the same magnitude, but in opposite directions. An example pair of opposite PE direction images can be seen on Figure 2.3. This means, that for every voxel $\mathbf{x}(x,y,z)$ there is a displacement d, so a voxel with the same intensity exists at the location $\mathbf{x}(x,y+d,z)$ and $\mathbf{x}(x,y-d,z)$ in the two acquired images respectively, if the PE direction is y. From the two images, one can calculate the distortion map $d(x,y,z)$ by non-linearly coregistering the voxels, with the constraint that the voxels only move in the PE direction, with the same magnitude but opposing direction.

[2]To be precise, the PE direction is the same, but the acquisition order of k-space rows is reversed (the blip directions are opposite)

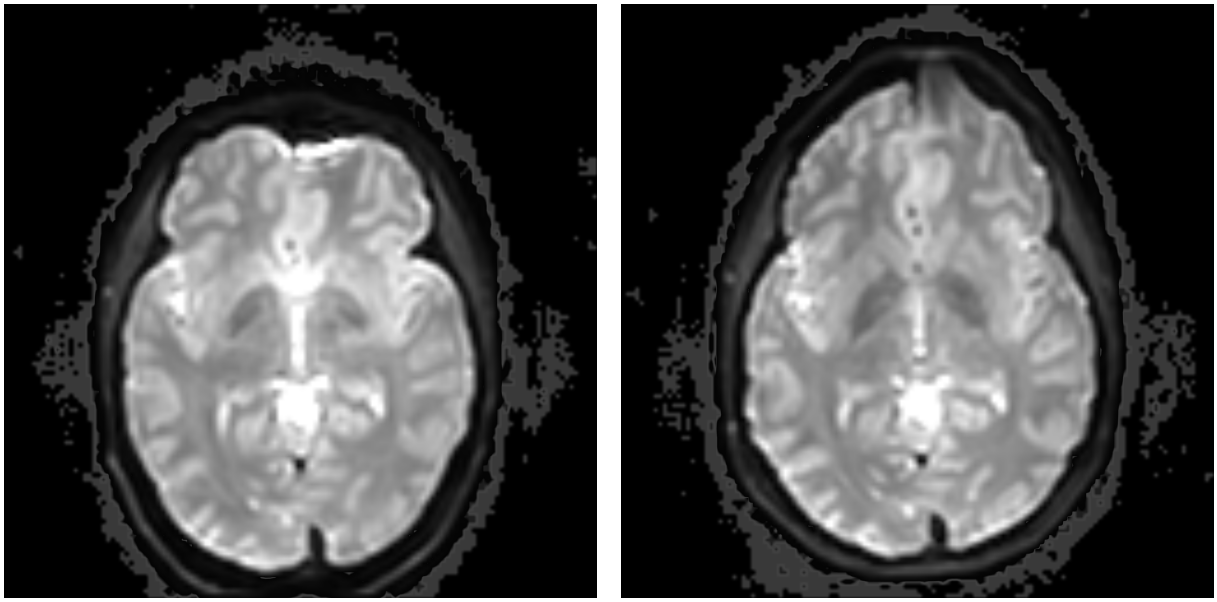

(a) (b)

Figure 2.3: An example SE-EPI image with Anterior-Posterior (a) and Posterior-Anterior (b) phase-encoding directions.

A field map in Hz can be calculated by

$$\Delta B_0(x,y,z) = d(x,y,z)/T_{\text{acq}}, \tag{2.5}$$

where T_{acq} is the total readout time for the SE-EPI sequence. The total readout time is the time it takes for one slice of the image to be read out, and can be calculated by

$$\text{EES} = \frac{1000 \cdot \text{WFS}}{\text{IF} \cdot 3.4 \cdot (\text{ETL}+1)}/\text{PRF} \tag{2.6}$$

and

$$T_{\text{acq}} = \text{EES} \cdot \text{ETL}, \tag{2.7}$$

where WFS is the water-fat shift, IF is the imaging frequency, ETL is the echo train length, PRF is the parallel reduction factor in plane, and EES is the effective echo spacing[10].

Voxel Displacement Maps

The amount of displacement caused by the field inhomogeneity can be calculated from the field map and the acquisition time,

$$\text{VDM}(x,y,z) = \gamma \Delta B_0(x,y,z) T_{\text{acq}}, \tag{2.8}$$

where T_{acq} is the readout time of a slice using the EPI sequence, and VDM for each voxel is the map of voxel shifts or Voxel Displacement Map.

2.5 Calculating activation maps

In order to calculate activation maps for a specific stimulus, a statistical analysis needs to be performed. The most common approach is setting up a general linear model (GLM) that contains the timing of the stimuli. The result is differentiated between two hypotheses[11]. The null hypothesis states that there is no correlation between the observed results and the task given to the subject. For every hypothesis based analysis, a p-score is calculated from the probability distribution of the statistic under the null hypothesis. If the p-score is smaller then a chosen threshold, the null hypothesis is rejected, and the results are deemed statistically significant. In task-based fMRI, the null hypothesis states that the area is unaffected by the task, and the areas where the null hypothesis is rejected are considered "active" under the given paradigm.

For calculating the responses, a GLM is fitted onto the measured data along the time dimension. The GLM is described by the equation:

$$Y = X\beta + \varepsilon, \tag{2.9}$$

where Y is the observed response, which is the linear combination of X, the explanatory variables in the design matrix, and β, the parameters of the model. ε is the fitting error of the model, which describes the variance coming from independent sources.

When fitting the model, a design matrix is constructed based on the paradigm (X), and the goal is to find a combination of the β parameters such that the error term gets minimized, when Y is the preprocessed functional data for a subject. The β values corresponding to the condition show the magnitude of the response for a given task. Activation maps can be constructed from these, after testing for statistical significance and spatial filtering based on cluster size.

2.6 Statistical analysis

First-level analysis

During first-level analysis, a GLM is fitted for every individual subject to calculate β values for every voxel.

After β values have been calculated for all explanatory variables, contrast levels can be set to differentiate the activation coming from different sources. A contrast map is created by multiplying the contrast vector by the β maps.

On the calculated contrast maps, a statistical significance test is done with a selected p significance level. Because every voxel needs to be tested individually, a large number of tests are required. When performing multiple statistical tests, the risk of type I errors rises, meaning that the chance of false positive results is increased. There are multiple ways to correct for these type of errors [12], but we only discuss Family-wise Error Rate correction (FWER-correction) here.

FWER is defined as the probability of obtaining at least one false positive in a set of tests. With FWER-correction, we can limit the occurrence of false positives in our analysis. For example, in a sample of 100 tests on average, a maximum of 5 may be false positives after FWER-correction at $p<0.05$ significance level.

Second-level analysis

After calculating the first-level analysis for all subjects, a group-level analysis can be done using the contrast maps from the first-level analysis. Multiple different statistical tests can be used, depending on the analysis. For example, by using a parametric t-test, an average activation map can be calculated for a group of subjects. After selecting the statistical test, a GLM is fitted, and group-level β values are calculated. After calculating the β values, significance levels can be set, and statistical significance can be tested.

2.7 Calculating Regions Of Interest (ROI) metrics

To study the effects of distortion correction on activation maps, we used *ICN_Atlas*[13]. With this toolbox, developed by Lajos Kozák et al., we can quantify fMRI activation patterns in relation to anatomical atlases. As an anatomical template, we used the Desikan-Killiany[14] parcellation (34 cortical ROIs per hemisphere) appended with 6 subcortical regions.

To quantify the spatial involvement and activation strength of a given ROI, a number of different metrics can be used, but we only mention a few that we used[13].

For calculating the relative spatial involvement of a given ROI, we used the formula

$$IR_i = \frac{|SPM_t \cap ROI_i|}{\sum_i |SPM_t \cap ROI_i|}, \tag{2.10}$$

where SPM_t is the thresholded activation map and ROI_i is the ith ROI in the atlas. This metric shows the ratio of the activated voxels in a given ROI over the total number of activated voxels in the activation map.

To quantify the significance of activation in a given ROI, we calculate the normalised mean ROI activation with the formula

$$MA_{N,i} = \frac{\sum_n \frac{\langle SPM_t \rangle_n \times ROI^B_{i,n} - min\langle SPM_t \rangle}{max\langle SPM_t \rangle - min\langle SPM_t \rangle}}{|SPM_t \cap ROI_i|}, \tag{2.11}$$

where $\langle SPM_t \rangle_n$ is the value of the nth voxel in the thresholded activation map, $ROI^B_{i,n}$ is the binarized version of the ith ROI in the selected atlas, $min\langle SPM_t \rangle$ is the activation threshold and $max\langle SPM_t \rangle$ is the peak statistical value of the activation map. In the equation, the numerator normalises the statistical values between the threshold value and the global maximum to the [0,1] interval, then it is divide by the number of activated voxels in ROI_i.

Chapter 3

Methods and materials

3.1 Data acquisition

At the Semmelweis University Medical Imaging Centre, functional MRI data were collected for 18 people in two groups on a 3T Philips Ingenia scanner. The first group consisted of 10 healthy young volunteers (average age 23.4 ± 4), while the second group consisted of 8 healthy young volunteers (average age 22.9 ± 1). All participants gave written informed consent prior to the examinations, and raw data was anonymized before processing. For the first group, three different paradigms were acquired: speech comprehension, picture naming, and finger tapping. For the second group, a verbal memory task was acquired in two sessions. For every volunteer, a T_1-weighted image, functional GRE-EPI images, and two GRE images with different echo-times were acquired. A High Angular Resolution Diffusion Imaging (HARDI) image was also acquired for the first group, from which the SE-EPI images with opposite PE directions were selected with $b = 0$ weighting. For the second group, a dedicated series of SE-EPI images with opposite PE directions were also acquired for calculating the field maps. These SE-EPI images had matching resolution, echo-train length, and in-plane acceleration to the GRE-EPI images. The acquisition parameters can be found in Tables 3.1 and 3.2.

Image	TR (ms)	TE (ms)	Flip angle (°)	Resolution
T_1-weighted	9.84	4.56	8	1 mm isotropic
GRE, short TE	28	2.589	30	3 mm isotropic
GRE, long TE	28	6.645	30	3 mm isotropic
GRE-EPI	1000	25	65	2.5 mm isotropic
HARDI	5216	102.6	90	2 mm isotropic
SE-EPI	4750	45	90	2.5 mm isotropic

Table 3.1: Acquisition parameters for the acquired data

Paradigm	Number of volumes	Acq. time (min:s)	Temporal resolution (s)
Finger tapping	498	8:33	1.03
Picture naming	384	6:39	1.03
Speech comprehension	384	6:39	1.03
Verbal memory	384	6:39	1.03

Table 3.2: Additional acquisition parameters for the functional GRE-EPI data

The additional parameters for calculating the total readout time for the EPI sequence, needed for the displacement map calculation, can be found in Table 3.3.

Parameter	Group 1	Group 2
WFS	17.7 ppm	17 ppm
IF	127.763 MHz	127.763 MHz
ETL	49	49
PRF	1.8	1.8

Table 3.3: The different parameters needed for calculating the total readout time for the EPI sequence for the different groups

3.2 Functional paradigms

Finger tapping task

During the finger tapping task, volunteers had 3 different instructions shown on an MRI compatible screen: 'left', 'right', and 'rest'. During 'left' and 'right', they had to touch their thumbs to their other fingers, on the hand shown on the screen. Between each active block, a passive block was placed, where the subject was instructed to remain still. The paradigm's block design can be seen on Figure 3.1.

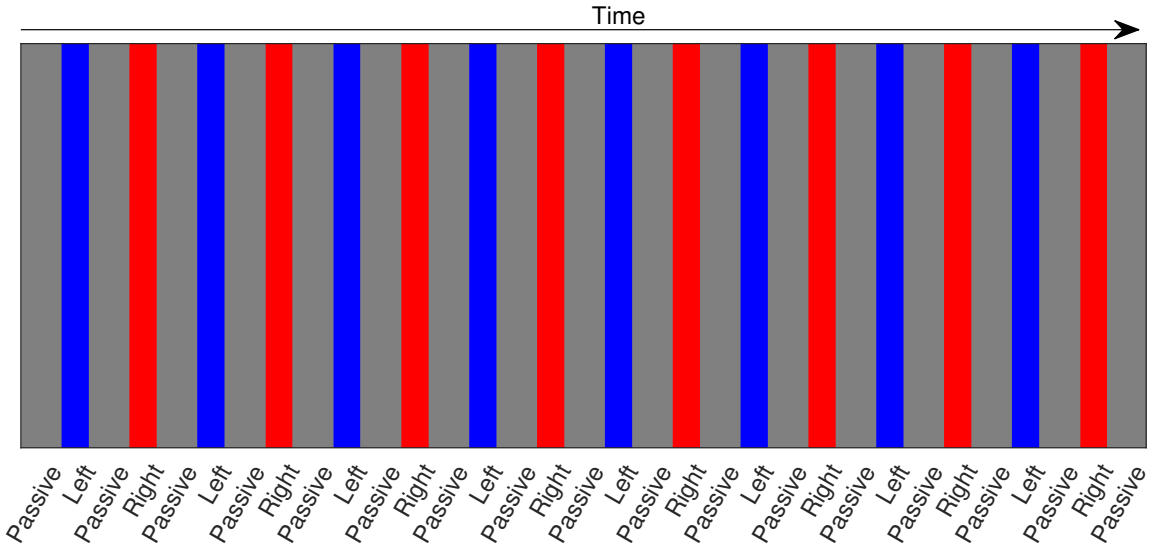

Figure 3.1: The block design of the finger tapping task. The greyed out lines are passive blocks, the blue and red lines are left and right active blocks, respectively. 18 volumes were acquired during the passive and 12 during the active blocks.

Picture naming task

During the active condition, volunteers saw either a living or an inanimate object, had to name it in their minds and press the right button if it was a living being, or the left if it was inanimate. During the passive condition, there were arrows on the screen, and the volunteers had to press the button on the side where the arrow was pointing. The paradigm's block design can be seen on Figure 3.2.

Speech comprehension task

During this task's active condition, volunteers had to listen to and comprehend a pre-recorded speech. During the passive condition, the reversed speech recording was playing. The subjects were instructed to listen passively. The paradigm's block design can be seen on Figure 3.2.

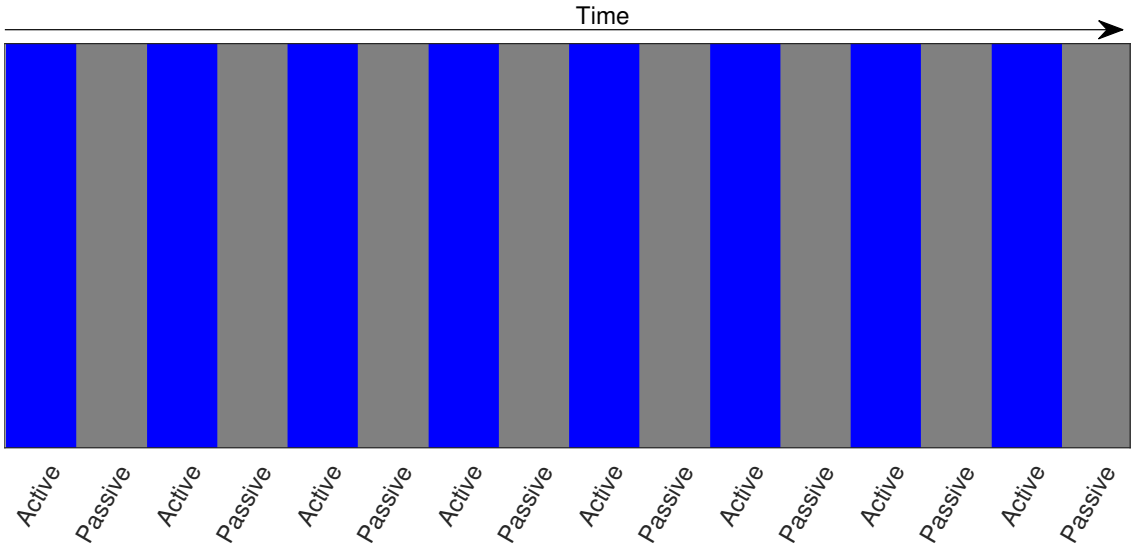

Figure 3.2: The block design of the speech comprehension and picture naming tasks. The greyed out lines are passive blocks, and the blue lines are active blocks. Both the active and passive blocks were 24 volumes long.

Verbal memory task

In preparation for the verbal memory task, a table of words were given to each volunteer. The table included 13 categories, each of which included 7 words that the volunteers had to learn in advance. During the task four different blocks repeated after each other. During the 'Old' block, a category from the learned list was shown on an MRI compatible screen, and the volunteers had to recall the words from the category. For each word recalled, a button had to be pressed. During the 'PressOnX' block, the letter X was shown on the screen with random timing, and for every X, the button had to be pressed once. The 'New' block showed a new, previously unseen category, and the volunteers had to come up with words fitting into that category. For every word, a button had to be pressed. The fourth block was a passive block, where the subject was asked to remain still and no task was given. The paradigm's block design can be seen on 3.3.

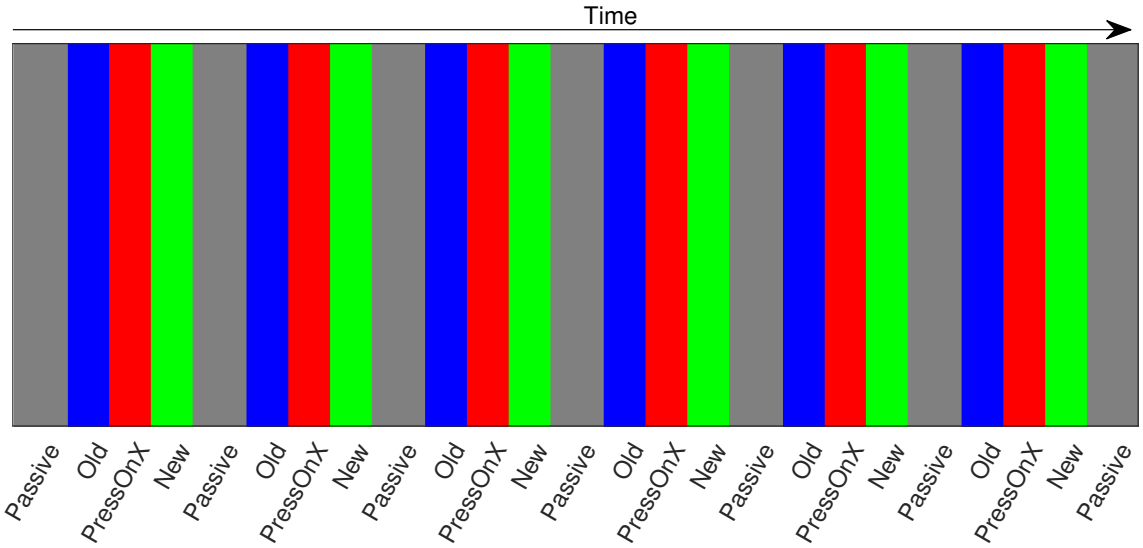

Figure 3.3: The block design of the verbal memory task. The greyed out lines are passive blocks, the blue lines are the 'Old' blocks where the learned words had to be recalled, the red lines are 'PressOnX' blocks, and the green ones are 'New' blocks. 18 volumes were acquired during the passive and 12 during the active blocks.

3.3 Data processing

For data processing, we used Matlab 2021a, with the licence provided by the Budapest University of Technology and Economics[15], and SPM12[16]. For calculating the VDMs for the DEPM-correction, we used SPM12's FieldMap toolbox. The FieldMap toolbox calculates the displacement maps following the steps described in Chapter 2.4, from the magnitude and phase data of the two GRE images acquired with different echo times. The toolbox first subtracts the two phase values voxel-by-voxel, then unwraps phase-jumps that might have occurred. After unwrapping, masking, and smoothing is performed before calculating the field map. An example field map can be seen on Figure 3.4.

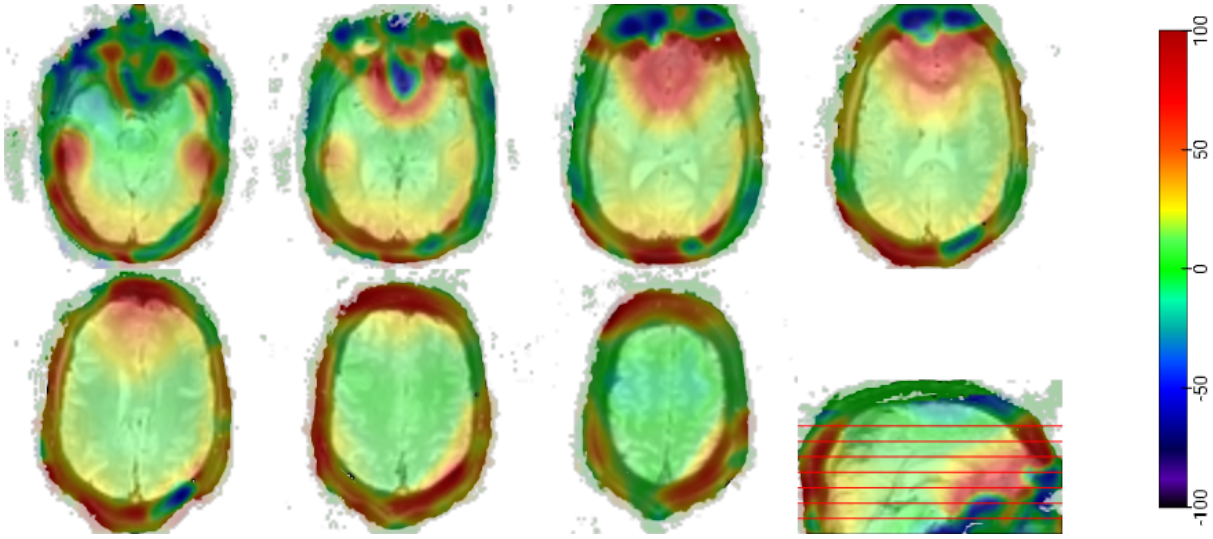

Figure 3.4: One example field map calculated using the FieldMap toolbox in Hz, overlayed on the functional image of a subject, in neurological convention (left side on left).

The calculated field maps change rapidly around the basis of the frontal lobe, as can be seen on Figure 3.4 (see images 1-2 in the first row from the left). We realized that the toolbox was unwrapping the phases incorrectly. Because merging a large number of regions during phase unwrapping caused errors, the published toolbox code limited the number of initial regions to 2. After increasing this number to 9, we managed to eliminate sharp changes in the field map. An example field map with 9 initial regions can be seen on Figure 3.5.

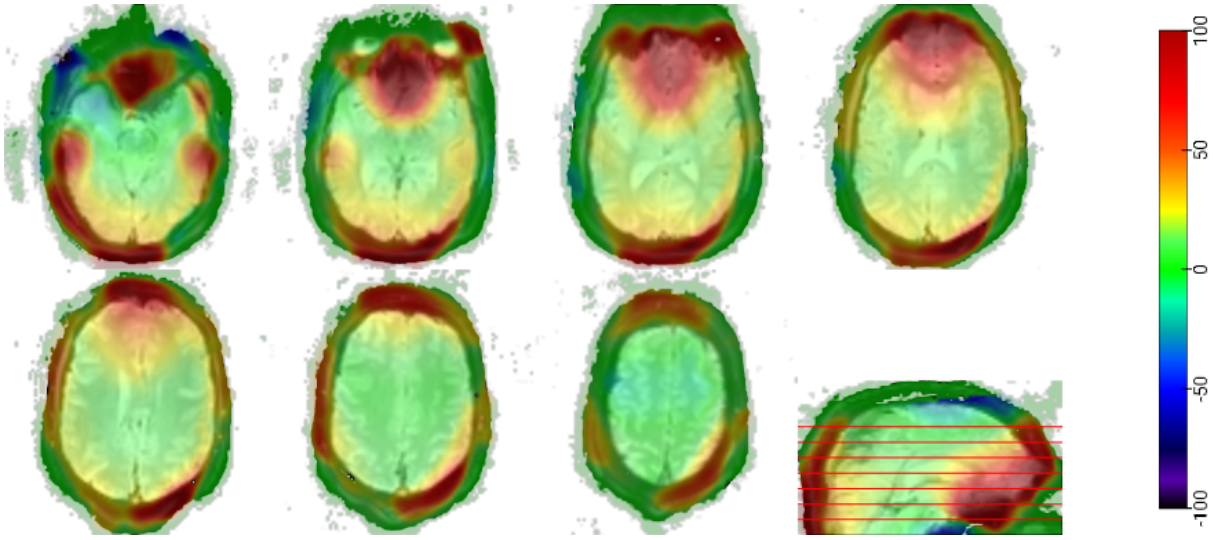

Figure 3.5: One example field map calculated with the number of initial regions set to 9, in Hz, overlayed on the functional image of the subject, in neurological convention (left side on left).

From these field maps, we calculated Voxel Displacement Maps by multiplying them with the total readout time, which we calculated using the values in Table 3.3 and Equations 2.6 and 2.7. The total readout time was $T_{\text{acq}} = 22.1642$ ms for the first group and $T_{\text{acq}} = 21.3041$ ms for the second group. After calculating the VDMs, the toolbox coregistered them to the functional data for a better fit.

For the OPED-correction, we had b=0 images from the HARDI sequence (OPED), and dedicated SE-EPI images for the second group of subjects (OPED-2). For processing these images, we used FSL's TOPUP [17] to calculate the field maps with the steps described in Chapter 2.4. After calculating the field maps, we put them into SPM12's FieldMap toolbox to calculate the VDMs.

To compare the VDMs resulting from the different methods, all VDMs of each subject were transformed into the same MNI-152 coordinate system. In order to quantify the distortion observed in different areas of the brain, we averaged the absolute values of the individual VDMs.

Before preprocessing the data, we resampled the T_1-weighted images to 2.5 mm isotropic resolution to decrease artificial variability when coregistering the functional data by decreasing the amount of interpolation needed.

For every volunteer and paradigm, we followed the same preprocessing pipeline implemented in an SPM batch script, which consisted of the following steps:

1. Realign & unwarp, once with DEPM-correction, once with OPED-correction, and once without distortion correction
2. Slice-timing correction
3. Segmentation of mean unwarped functional image (grey matter, white matter, cerebrospinal fluid, deformation field calculation to MNI-152 coordinate system)
4. Normalisation of functional data to MNI-152
5. Segmentation of anatomical image (grey matter, white matter, cerebrospinal fluid, deformation field calculation to and from the MNI-152 coordinate system)
6. Inverse normalisation of the functional images with the inverse deformation field to non-linearly coregister the data to the anatomical scans
7. Smoothing of functional images by convolution with a Gaussian kernel (FWHM=6 mm)

We investigated the differences in geometric distortion between the anatomical images and the mean unwarped functional images by coregistering them to each other and calculating the Normalised Mutual Information values.

3.4 Statistical analysis

Calculating individual activation maps

After preprocessing, we used a first-level analysis to calculate the β values for every voxel. For the speech comprehension and picture naming tasks, we set Active>Rest contrast to see the activation, and for the finger tapping task, we set Left+Right>Rest to see the activation in both hemispheres together. For the verbal memory task, the contrast was set to Old+New>PressOnX to see the activation in regions related to verbal memory and speech production without the regions related to pressing the button. After defining contrasts, we checked which voxels had significant activation ($p<0.05$ with Family Wise Error Rate correction).

Group-level activation maps

Because we calculated the activation maps in the individual coordinate systems of every subject, we normalised the contrast maps to MNI-152 space using the deformation fields (calculated in preprocessing step 5) before group-level analysis.

For calculating group-level activation maps, we used a parametric t-test at a significance level of $p<0.001$ and cluster size thresholds of at least 5 voxels. After binarising these activation maps, we calculated the Dice-Sorensen (Dice) coefficients[18] to compare how similar the different activation maps were with and without distortion correction for every paradigm.

Comparing effects of inhomogeneity correction

After calculating the activation maps for all paradigms with and without the different B_0 inhomogeneity corrections, we used *ICN_atlas* to determine which brain regions were significantly activated, how significant the activation was, and how these regional activations were affected by the different distortion corrections. We selected a modified version of the Desikan-Killiany Atlas [14], parcellating the grey matter into 40 ROIs per hemisphere. We calculated the relative spatial involvement for all 80 ROIs on the group-level activa-

tion maps, with Equation 2.10 and examined those that had a value greater than 0.1. We calculated the normalised mean activation for the selected ROIs with Equation 2.11, and we compared the values for the different preprocessing methods involving inhomogeneity corrections.

Chapter 4

Results

Figures were created using MRIcroGL[19] with the built in standard MNI-152 template. All images are in neurological convention (i.e., the left side of the brain is on the left side of the image). For identifying different areas of the brain, we used MRIcroGL's built in AAL atlas[20].

4.1 Inhomogeneity correction

Voxel Displacement Maps

The average of the absolute value of the VDMs resulting from the three different inhomogeneity corrections (DEPM, OPED, OPED-2) can be seen on Figures 4.1 a), b), c). For all three inhomogeneity correction strategies, the figure shows the distortions mainly happen in the frontal, temporal, and occipital regions of the brain. The estimated magnitude of field inhomogeneity induced voxel shift increased across the different estimation methods, with DEPM correction producing the smallest shifts and OPED-2 correction producing the largest.

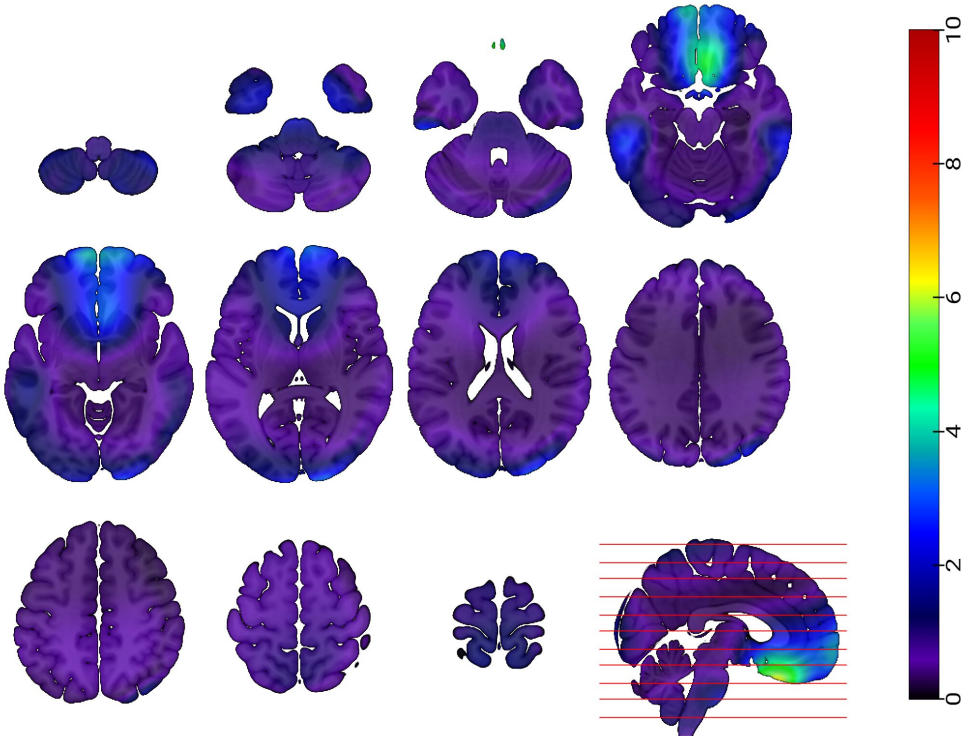

(a) Dual-echo Phase Mapping

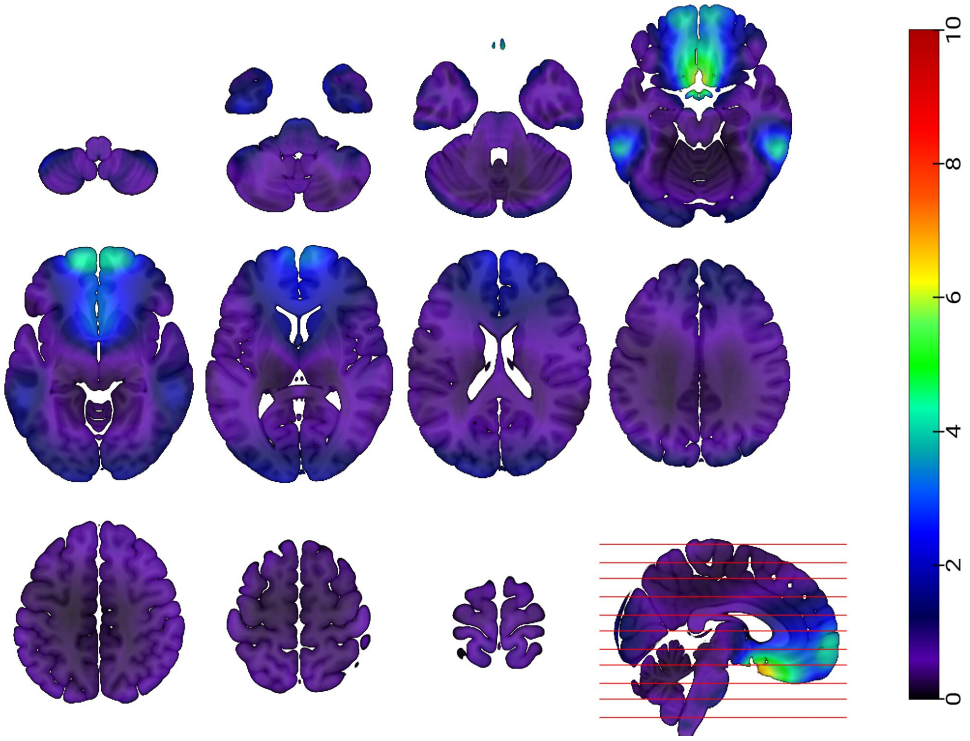

(b) Opposite PE Direction based VDMs (based on HARDI b=0 images)

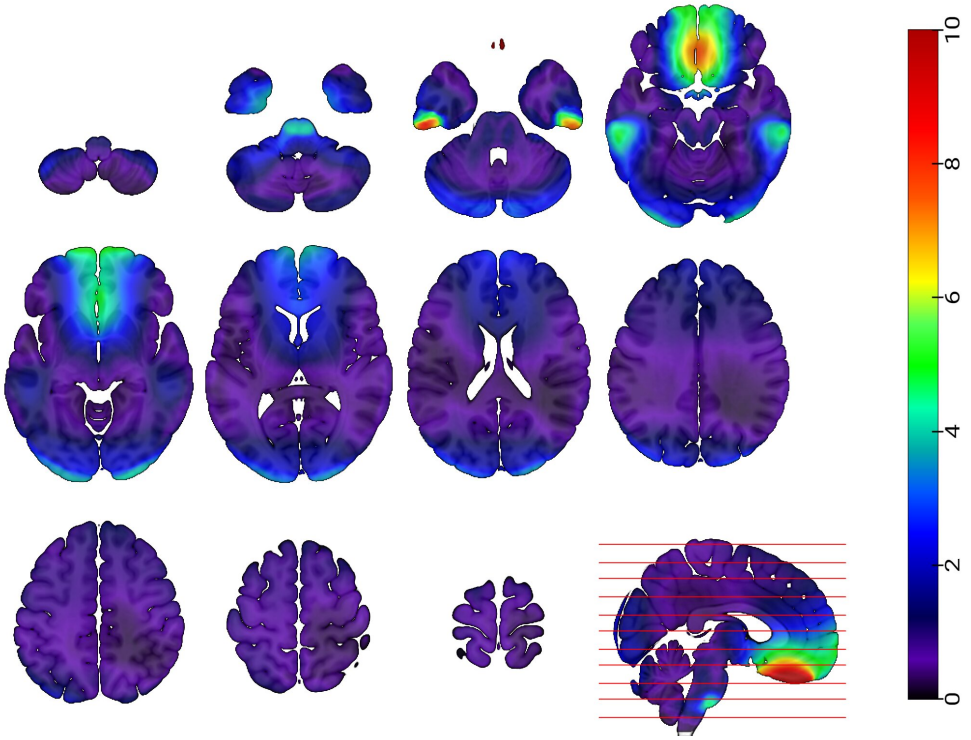

(c) Opposite PE Direction based VDMs (based on separate SE-EPI images)

Figure 4.1: The averaged Voxel Displacement Maps resulting from different field map calculation methods. All images show substantial displacements happen in the frontal, temporal, and occipital lobes. It can also be seen that the separate SE-EPI acquisitions estimate larger distortions around these parts.

Coregistration to the anatomical image

The Normalised Mutual Information values between the mean functional image after unwarping and the anatomical image with the different types of corrections (no correction, DEPM, OPED) for the different paradigms are shown on Figure 4.2.

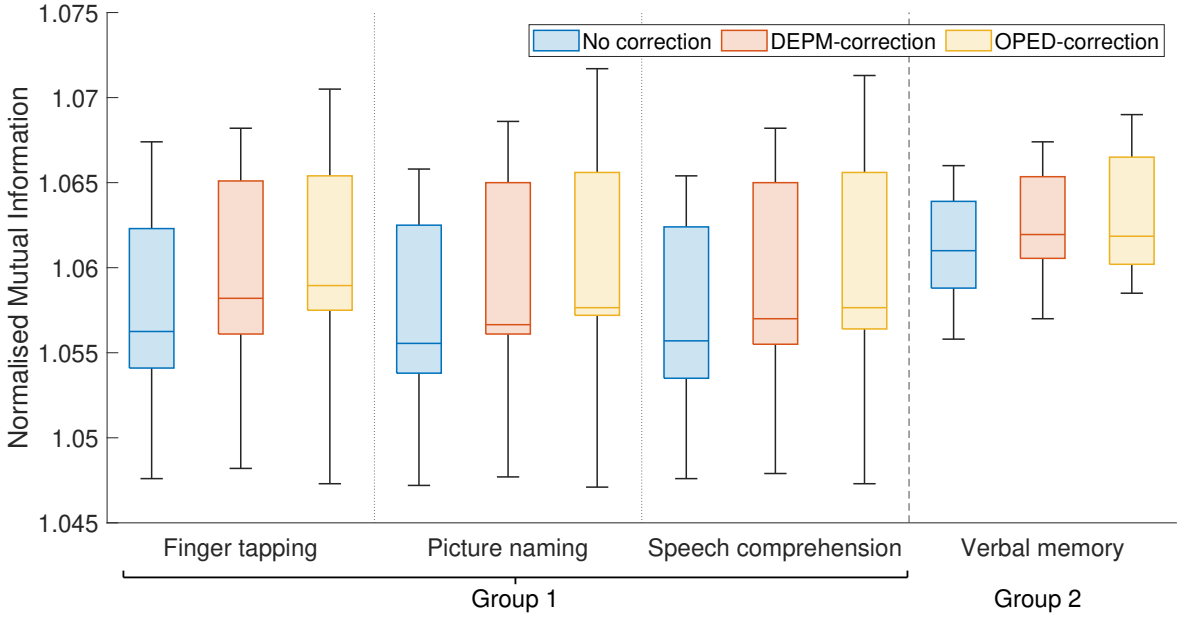

Figure 4.2: The Normalised Mutual Information values between the mean functional image and the anatomical image with different inhomogeneity corrections (No correction, DEPM, OPED) for the different paradigms.

The median NMI values increased with the use of all inhomogeneity correction strategies for all paradigms. The coregistration showed higher values when using the OPED-correction compared to the DEPM-correction. It can also be seen that the OPED-correction resulting from the separate SE-EPI measurements also resulted in higher NMI values for the verbal memory task.

4.2 Group-level activation maps

The activation maps for the finger tapping, picture naming, and speech comprehension paradigms without correction, with DEPM-correction, and OPED-corrections are shown on Figures 4.3, 4.5, and 4.7. For the activation maps calculated with different inhomogeneity corrections, we overlaid the outline of the activation clusters from the original, uncorrected activation map. A detailed version of Figures 4.3, 4.5, and 4.7 is included in Appendix A. Dice coefficients are reported to two decimal places, as the uncertainty of the overlap estimates does not justify higher numerical precision for the present sample size.

Finger tapping task

The activation maps for the finger tapping task without, with DEPM and with OPED-corrections are shown on Figure 4.3 a), b), and c). All activation maps show activation in the post- and precentral gyri in both hemispheres, the supplementary motor area, in parts of the cerebellum, and in the bilateral putamen.

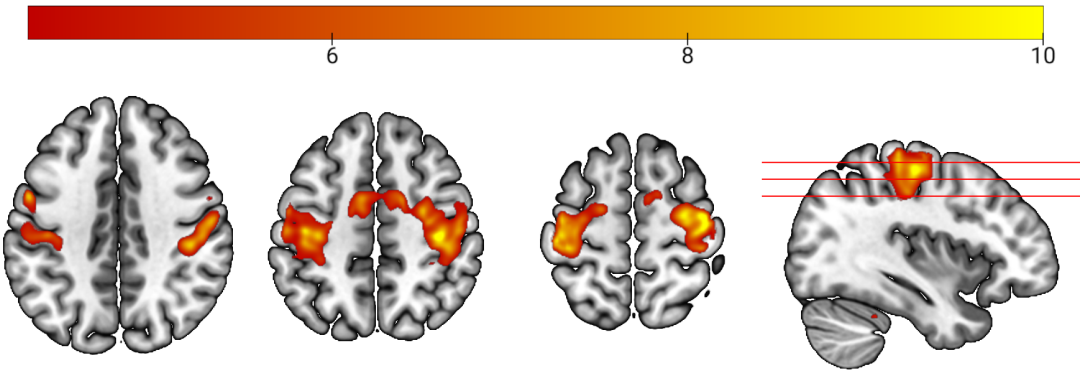

(a) No correction

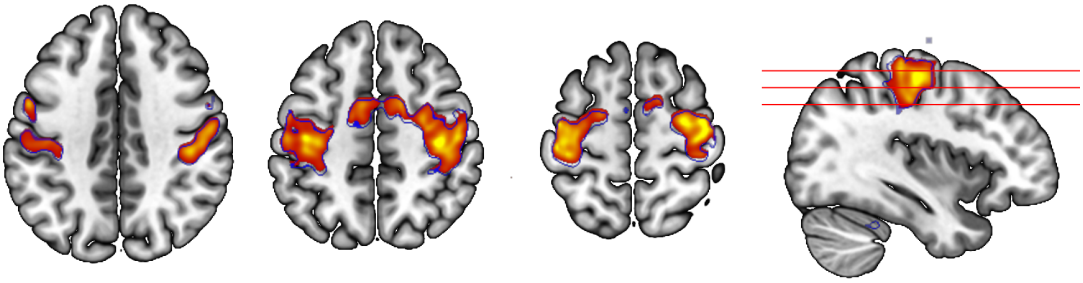

(b) With DEPM-correction

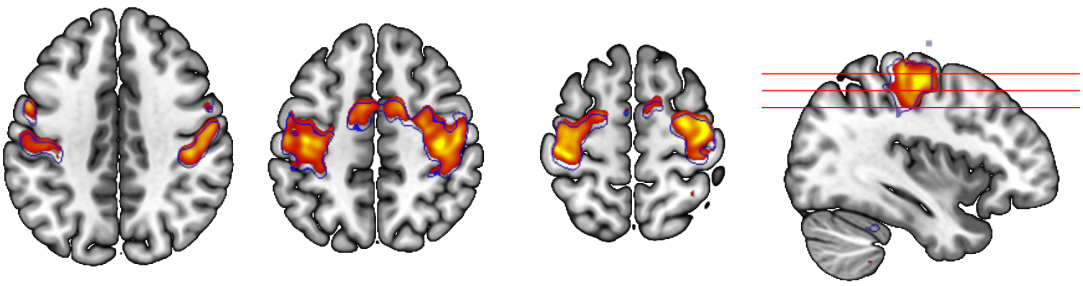

(c) With OPED-correction

Figure 4.3: Group-level activation maps resulting from the finger tapping task. Voxels with $p<0.001$ significance level are highlighted with red to yellow, overlayed on the MNI-152 template. On (b) and (c), the outline of the clusters from the original, uncorrected activation map is overlayed in blue. All activation maps show activation in the post- and precentral gyri on both sides and the supplementary motor areas.

The calculated Dice coefficients between the different activation maps are shown on Figure 4.4.

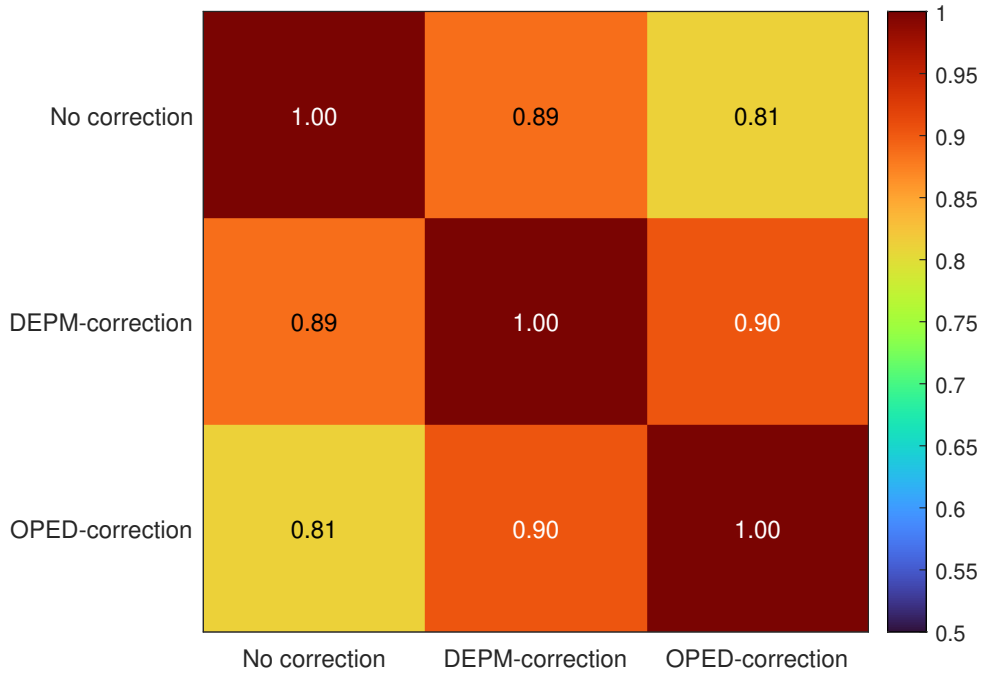

Figure 4.4: The calculated Dice coefficients for the finger tapping task between the different correction methods.

Picture naming task

The activation maps for the picture naming task without, with DEPM and with OPED-corrections are shown on Figure 4.5 a), b), and c). All activation maps show activation bilaterally in the fusiform gyri, in the middle and inferior occipital lobes, the supplementary motor area, and the precentral gyri. There is activation bilaterally in the frontal inferior triangularis area, the frontal inferior operculum, the putamen, and the insular cortices, but the activation is stronger in the left hemisphere.

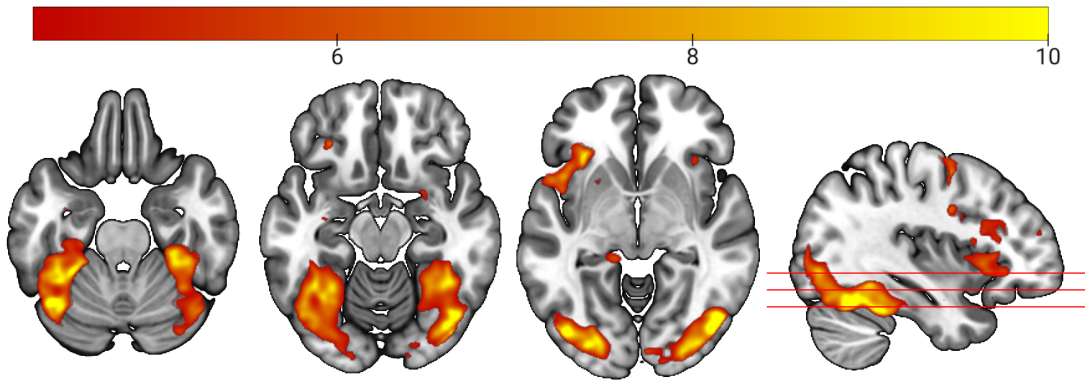

(a) No correction

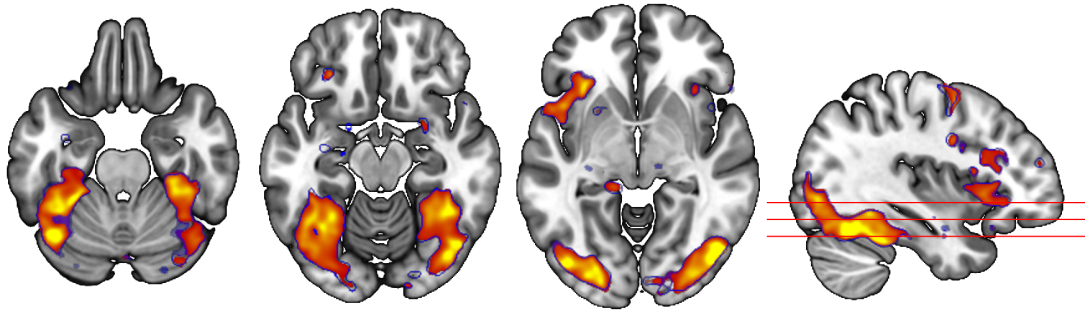

(b) With DEPM-correction

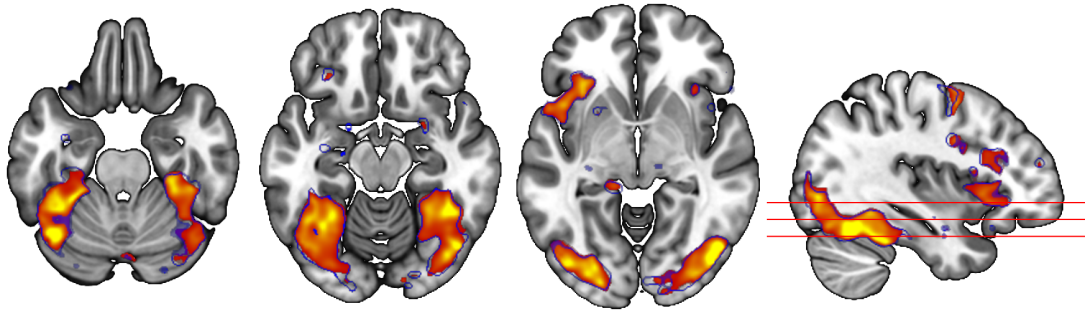

(c) With OPED-correction

Figure 4.5: Group-level activation maps resulting from the picture naming task. Voxels with $p<0.001$ significance level are highlighted with red to yellow, overlayed on the MNI-152 template. On (b) and (c), the outline of the clusters from the original, uncorrected activation map is overlayed in blue. The activation maps show activation bilaterally in the fusiform gyri and in the middle occipital and inferior occipital lobes.

The calculated Dice coefficients between the different activation maps are shown on Figure 4.6.

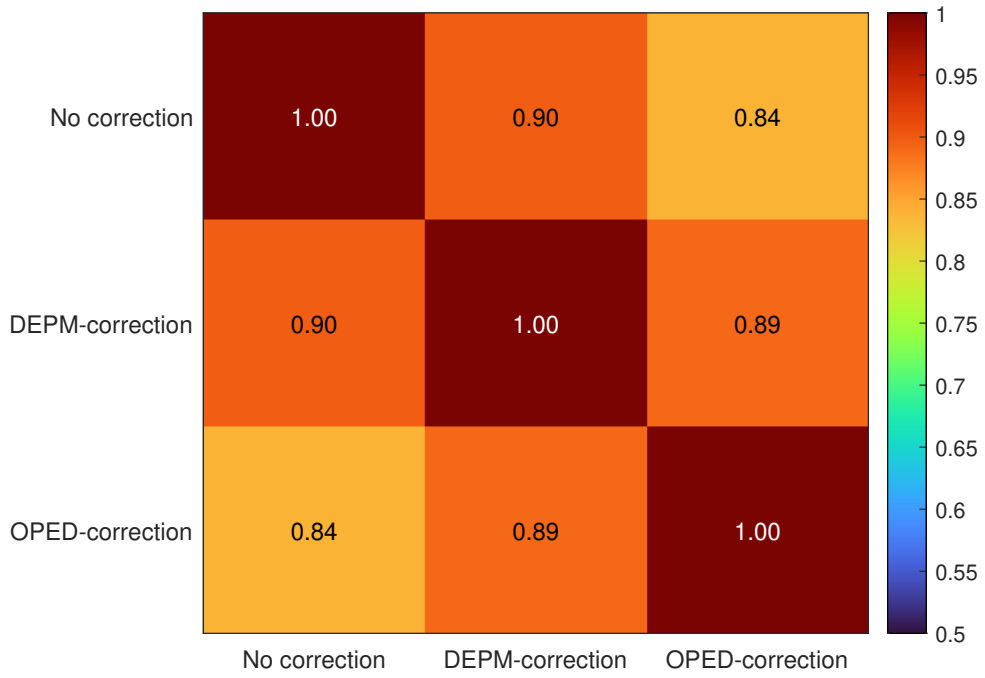

Figure 4.6: The calculated Dice coefficients for the picture naming task between the different correction methods.

Speech comprehension task

The activation maps for the speech comprehension task without correction, with DEPM and with OPED-corrections are shown on Figure 4.7 a), b), and c). All activation maps show activation in both hemispheres in the middle temporal gyri, with stronger and more extensive activation in the left hemisphere, in the hippocampi, and in the temporal poles in both hemispheres.

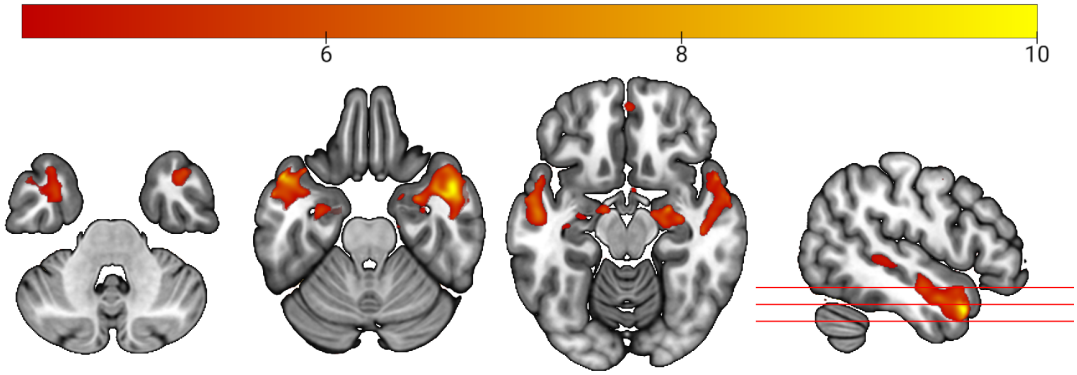

(a) No correction

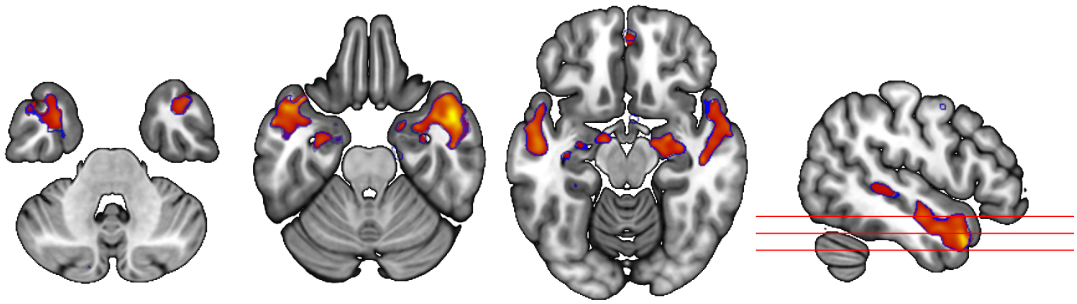

(b) With DEPM-correction

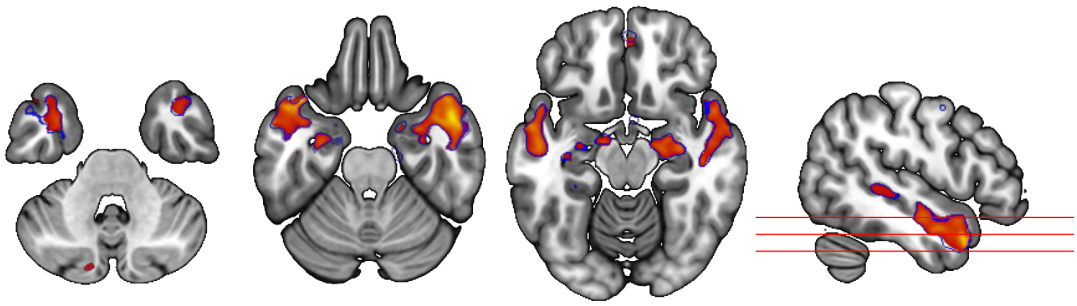

(c) With OPED-correction

Figure 4.7: Group-level activation maps resulting from the speech comprehension task. Voxels with $p<0.001$ significance level are highlighted with red to yellow, overlayed on the MNI-152 template. On (b) and (c), the outline of the clusters from the original, uncorrected image is overlayed in blue. All activation maps show activation in the bilateral middle temporal gyri, with stronger activation in the left hemisphere, in the bilateral hippocampus, and in the temporal poles.

The calculated Dice coefficients between the different activation maps are shown on Figure 4.8.

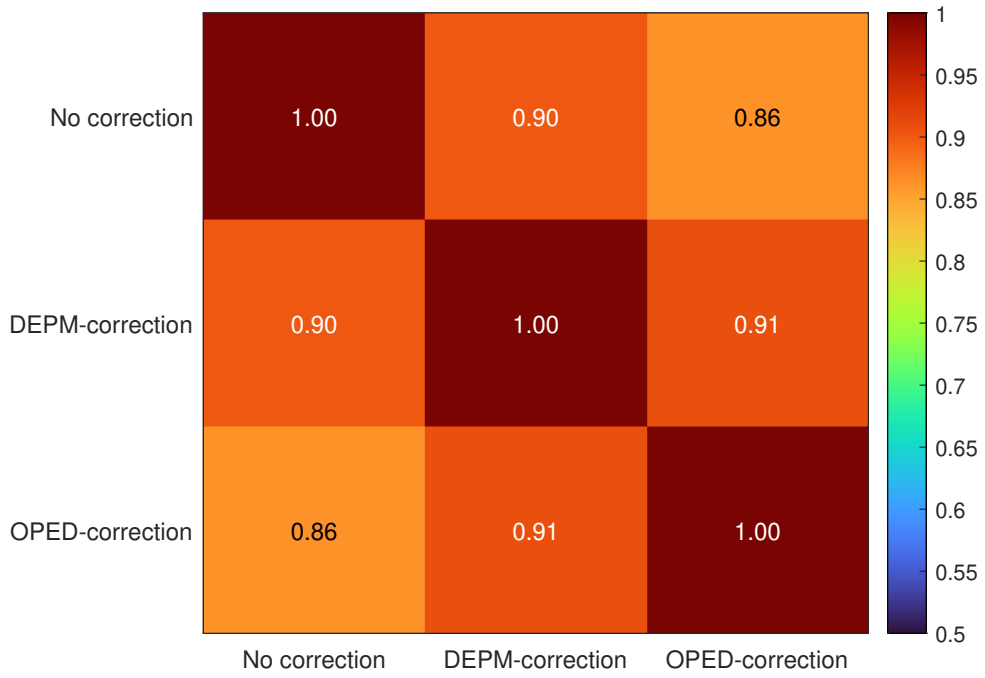

Figure 4.8: The calculated Dice coefficients for the speech comprehension task between the different correction methods.

4.3 Verbal memory task

The group-level activation map of the verbal memory task without inhomogeneity correction is shown on Figure 4.9.

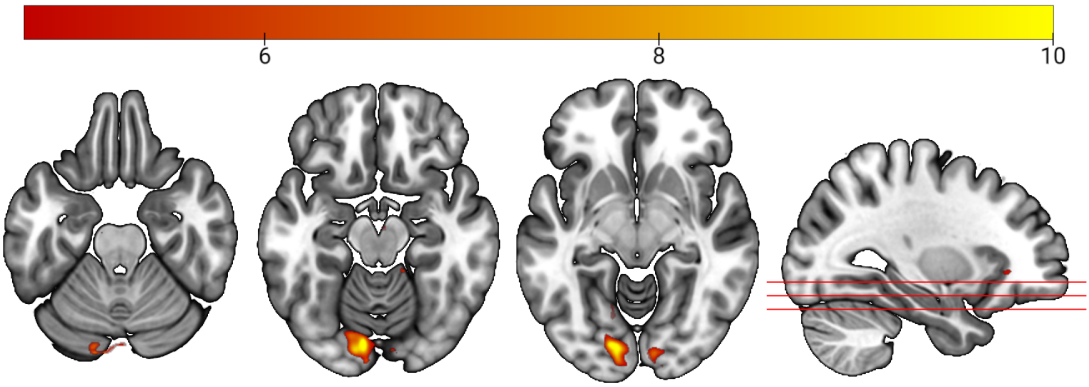

Figure 4.9: The group-level activation map for the verbal memory task without inhomogeneity correction. Voxels with $p<0.001$ significance level are highlighted with red to yellow, overlayed on the MNI-152 template.

In case of the verbal memory task with our selected contrast (Old+New>PressOnX), we expect activations in the bilateral hippocampi and the areas associated with speech production. An example of the expected activation map is depicted on Figure 4.10.

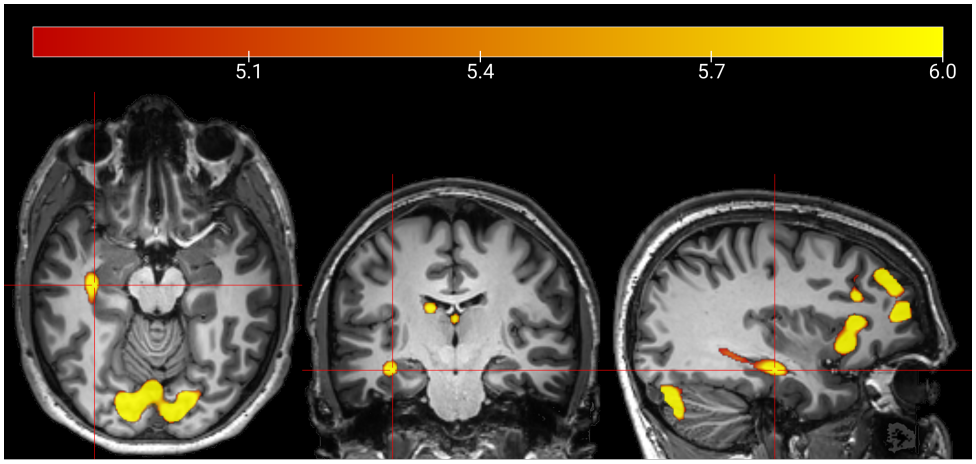

Figure 4.10: Subject-level activation map resulting from the verbal memory task with $p < 0.05$ significance level with FWER correction, overlaid on the subject's T_1-weighted anatomical image. The cursor indicates the expected activation related to memory function in the left hippocampus.

However, this subject-level activation result is an outlier among our results. Most calculated individual activation maps did not display the hippocampal activation suitable for localizing verbal memory functions. Our aim was to examine the effects of inhomogeneity correction on the expected hippocampal activation, but based on our results, we could not quantify this effect.

4.4 Effect of inhomogeneity correction

The normalised mean activation values for the ROIs with group-level relative involvement higher than 0.1 for the finger tapping, picture naming, and speech comprehension task can be seen on Figures 4.11, 4.12, and 4.13, respectively. The choice of threshold for IR_i is arbitrary and was chosen as 0.1 to examine only those ROIs which have the most contribution in the activation map.

Finger tapping task

The ROIs with high IR_i for the finger tapping task include the left and right post- and precentral gyri. For the bilateral postcentral gyri, a decrease in the median activation strength can be seen with the DEPM and OPED-corrections, and a slight rise can be seen in the bilateral precentral gyri when either inhomogeneity correction is applied. The range of the activation strengths remains unchanged by the corrections.

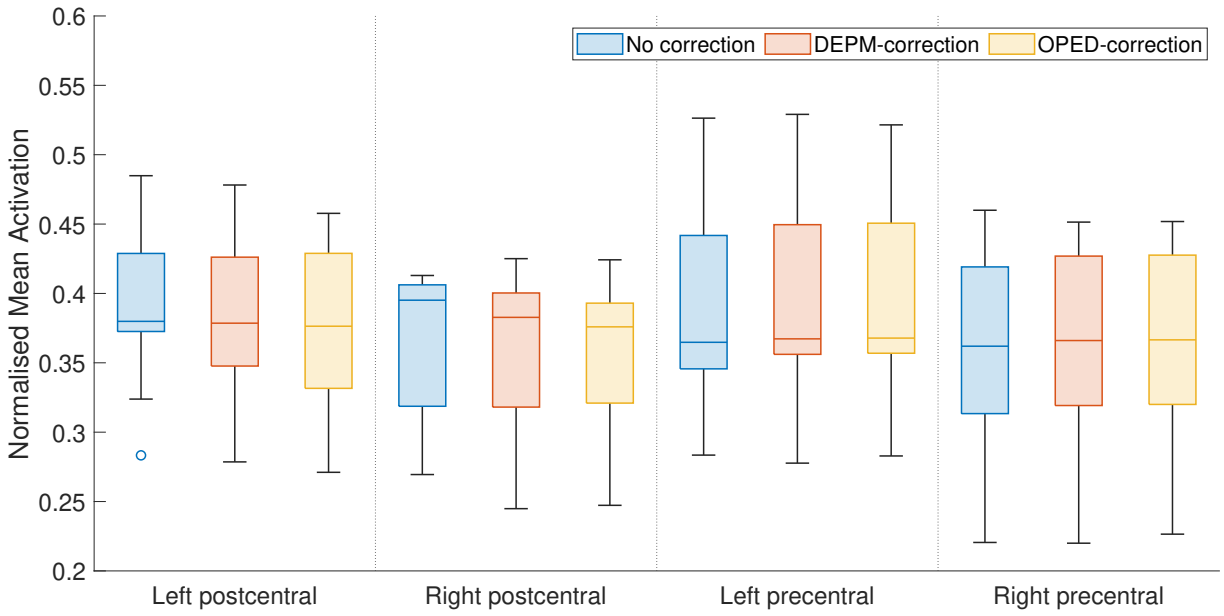

Figure 4.11: The $MA_{N,i}$ values for the left and right post- and precentral gyri for the three different correction methods. A decrease in median activation strength can be seen in the postcentral gyri bilaterally, and an increase can be seen in the precentral gyri if either correction is applied.

Picture naming task

The ROIs with high IR_i for the picture naming task include the left and right fusiform and lateral occipital gyri. The medians for the different correction methods did not show significant change, but the activation strength in some subjects increased in the left and right fusiform gyri when using the OPED-correction, as indicated by the changes in the range of the data.

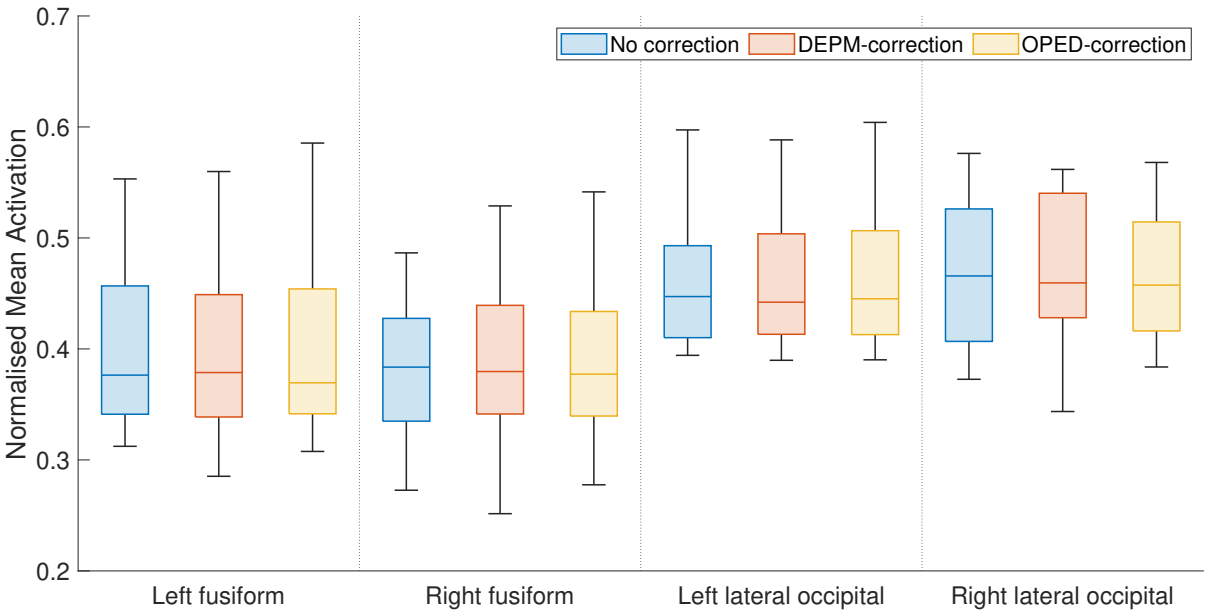

Figure 4.12: The $MA_{N,i}$ values for the left and right fusiform and lateral occipital gyri for the three different correction methods. The medians do not show significant change, but a slight increase in activation strength can be seen in the left and right fusiform gyri when using the OPED-correction.

Speech comprehension task

The ROIs with high IR_i for the speech comprehension task include the left and right middle temporal and superior temporal gyri. In the right middle temporal and right superior temporal gyri, a decrease in median activation strength can be seen when using the OPED-correction. In the left middle temporal and the left superior temporal gyri, an increase in activation strength can be seen for some subjects, when using the OPED-correction, as indicated by the changes in the range of the data.

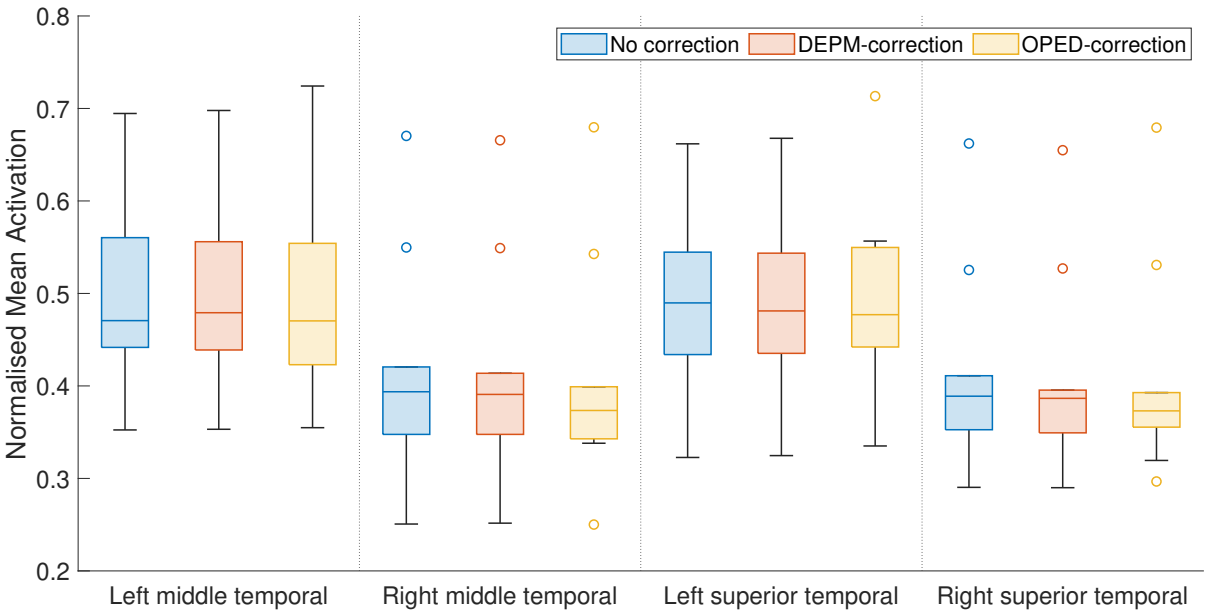

Figure 4.13: The $MA_{N,i}$ values for the left and right middle temporal and superior temporal gyri for the three different correction methods. The right middle and superior temporal gyri show a decrease in activation strength when using the OPED-correction. In the left middle and superior temporal gyri, the activation strength increases for some patients when using the OPED-correction, as indicated by the changes in the range of data.

Chapter 5

Discussion

5.1 Inhomogeneity correction

Voxel displacement maps

The average Voxel Displacement Maps confirmed that the largest susceptibility-related distortions occurred in the basal regions of the frontal lobes, in the temporal and occipital areas. These regions are located near air-filled cavities of the skull, like paranasal sinuses and ear canals, which cause sharp changes in local magnetic susceptibility. It can also be seen that the VDMs calculated from the new separate SE-EPI acquisitions estimate bigger distortions in these regions. This may be caused by the difference in the type of acquisition. The separate SE-EPI acquisition was matched to the functional acquisition in terms of slice-thickness, echo train length, and in-plane acceleration, while the HARDI b=0 images were not. The echo times were also closer to the functional echo times in case of the separate SE-EPI images, resulting in a better match between their contrasts (functional TE=25 ms; SE-EPI TE=45 ms; HARDI TE=102 ms). As a result, we expect the separate SE-EPI images to better quantify the distortion of the functional images than our previous methods.

Coregistration to the anatomical image

For comparing the effect of correction on the raw functional images, we quantified their "distance" from the anatomical scans. Normalised Mutual Information values were calculated between the mean functional image after unwarping and the T_1-weighted anatomical image. The median NMI values showed an increase when using either the DEPM or the OPED-correction in all paradigms, but the OPED-correction showed higher values. A higher NMI value means a closer fit between the two images, so by correcting the distortions caused by the field inhomogeneities, the functional image matched the anatomical image better.

Higher NMI values were present when we used the OPED-correction resulting from the separate SE-EPI correction. All this confirms our expectation that we will get better

inhomogeneity correction if the SE-EPI sequence is matched to the functional measurements.

5.2 Group-level activation maps

The analysis of the obtained group-level activation maps without and with the two inhomogeneity corrections showed the expected activation patterns for each paradigm [21].

The finger tapping task showed bilateral activation in the pre- and postcentral gyri, the primary motor and sensory cortices, as well as the supplementary motor areas. Furthermore, we found activation in the bilateral putamen and the cerebellum: areas all associated with motor function. The location of activations stayed roughly the same for the different preprocessing methods, but activation patterns shifted in the anterior direction in the post- and precentral gyri when using either the DEPM or the OPED-correction. From the Dice coefficients, it can be seen that the original activation map without correction had a similarity of 89% with the correction resulting from DEPM, and a similarity of 81% with the correction resulting from OPED. This means that the OPED-correction not only estimated and corrected for bigger distortions on the raw functional images, but these effects translated to bigger shifts in the activation patterns as well. Still, the Dice coefficient remains over 80%, indicating that detected areas largely overlap with or without correction.

In the picture naming task, activation was observed in the middle occipital and inferior occipital cortices, and the bilateral fusiform gyri, areas that process visual information. Activation was also observed in the frontal inferior operculum and the frontal inferior triangularis area, overlapping with Broca's area, the motor center of language processing. The calculated Dice coefficients show an 90% similarity between the original activation map and the correction using the DEPM-correction, and an 84% similarity between the original and the OPED-corrected activation map. This confirms that the OPED-correction estimates and corrects larger distortions than DEPM, while patterns again largely overlap with the uncorrected results.

For the speech comprehension task, activation was localised in the bilateral middle temporal gyri, the temporal poles, and the hippocampi, which are associated with processing auditory information. The Dice coefficients showed a 90% similarity between the original and the DEPM-corrected images and an 86% similarity between the original and the OPED-corrected images, yielding the same result for the third paradigm. The larger overall Dice coefficients point to the main anterior-posterior direction of the correction. Even though the temporal activations are close to the ear canals and mastoid bones, the

activated areas run along the anterior-posterior direction and not perpendicularly, as e.g., the primary motor cortices.

Activation maps only showed activation with a lower significance threshold ($p<0.001$), only a few voxels remained significant after correcting for family-wise error rate at $p<0.05$ significance level. We believe that this is due to low statistical power, which results from the small number of subjects in our study. Nevertheless, at a lower significance threshold, the results met our expectations, both without and with correcting for B_0 field inhomogeneities.

5.3 Verbal memory task

We included the verbal memory task in this thesis because it is an important step in the surgical planning for patients with temporal lobe epilepsy. As we showed earlier, the temporal lobe suffers from geometric distortions due to inhomogeneity, resulting in displacements of the activation patterns and decisively influencing surgery planning. We collected data for 8 healthy young volunteers, who all learned a given list of words a day before the acquisition. Unfortunately, not all volunteers showed the expected hippocampal activation during the task. Thus, the effect of distortion correction on group-level hippocampal activations could not be examined. Individual assessment of the activation maps is a rigorous task and is beyond the scope of this thesis.

5.4 Effect of inhomogeneity correction in selected ROIs

When looking at the $MA_{N,i}$ values for the selected ROIs ($IR_i > 0.1$), median group differences were slight. On subject-level, however, we found individual differences in activation strength in the selected ROIs with and without corrections. Such increases and decreases in activation strength are the results of voxel shifts and amplitude modulation caused by the corrections. We believe sensitivity of the activation localisation is increased on the individual level, by potentially filtering out false positive activations and enhancing true positive ones. Statistical power of our group-level analyses could be enhanced by including more subjects in the study.

For the finger tapping task, the ROIs with high relative involvement include the bilateral post- and precentral gyri. The median normalised mean activation values for the postcentral gyri decreased, while the values for the precentral gyri increased, when using either inhomogeneity correction method. These regions are next to each other in the anterior-

posterior direction, so we interpret our results as a slight forward shift in the activation patterns due to the inhomogeneity corrections.

For the picture naming task, the effects of the correction were not as striking, but using the OPED-correction had effects in the left and right fusiform gyri. Some subjects showed increased activation strength in these areas, while the same could not be said about the lateral occipital regions that are located farther situated from the ear canals. We interpret these results as an example of increasing sensitivity in individual cases, but further subjects are needed to be tested for confirmation.

Using the OPED-correction for the speech recognition task resulted in decreased median activation strength in the selected ROIs, with the exception of a few subjects. These subjects showed increased activation strength in the left middle and superior temporal gyri, and reduced activation strength in the right middle and superior temporal gyri. Both the group-level effect and the individual alterations are small, a larger control group should be evaluated for greater statistical power.

Chapter 6

Conclusion

In this thesis, we investigated the effect of two B_0 inhomogeneity correction methods on task-based fMRI activation maps. Using functional MRI data of two groups of healthy subjects, we investigated four different paradigms (finger tapping, picture naming, speech comprehension, and verbal memory) and we evaluated how the different corrections affect raw fMRI data, individual and group-level activation maps.

Based on Normalised Mutual Information between mean functional and anatomical images, we can say that corrections brought these images meaningfully closer to each other. We obtained the largest NMI values, thus the best functional-anatomical alignment with the OPED-correction based on the separate SE-EPI images.

Evaluating group-level activation maps of three of the four paradigms (finger tapping, picture naming, speech comprehension), we found measurable differences between the activation maps without and with both inhomogeneity corrections. We believe changes in the paradigm-specific activation maps reflect improvement in the accuracy of spatial localisation, as we showed that raw functional images became better aligned to the anatomical data through inhomogeneity corrections. Opposing Phase Encoding Direction-correction yielded larger shifts of activation patterns than the Dual-Echo Phase Mapping method. The localisation of task-related brain activations is reliable and clinically relevant even without inhomogeneity correction, but the accuracy and statistical power is imporved by correction methods. The most convincing results were obtained with the OPED-correction based on the separate SE-EPI images.

The effects of inhomogeneity correction were not uniform for all paradigms and brain regions. Voxels with task-related signal changes may shift between regions of interest as a result of inhomogeneity correction, and the nonlinear nature of the correction affects signal amplitudes, resulting in increased or reduced activations in certain areas. Further modified paradigms and repeated measurements are needed to assess the sensitivity of activation localisation with or without inhomogeneity corrections.

The verbal memory paradigm did not show significant activation in the expected hippocampal area for most subjects, so the effect of inhomogeneity correction could not be examined for this paradigm. A new, different memory paradigm is currently under testing

at the Medical Imaging Centre, with a goal of finding the hippocampal activation reliably in all patients.

In summary, our findings confirm that incorporating B_0 inhomogeneity correction into the preprocessing pipeline of fMRI data enhances spatial accuracy and interpretability of activation maps, especially in regions prone to susceptibility artefacts.

Future work should include larger sample sizes, examinaton of additional paradigms, and the evaluation of advanced correction methods to further refine the correction of susceptibility-induced distortions during the analysis of our fMRI-data.

Chapter 7

Bibliography

[1] Daniel A. Orringer, David R. Vago, and Alexandra J. Golby. Clinical applications and future directions of functional MRI. *Seminars in Neurology*, 32(4):466–475, September 2012. ISSN 1098-9021. doi: 10.1055/s-0032-1331816.

[2] Russell A. Poldrack, Jeanette A. Mumford, and Thomas E. Nichols. *Handbook of Functional MRI Data Analysis*. Cambridge University Press, Cambridge, 2011. ISBN 978-0-521-51766-9. doi: 10.1017/CBO9780511895029.

[3] Marco Giannelli, Stefano Diciotti, Carlo Tessa, and Mario Mascalchi. Characterization of Nyquist ghost in EPI-fMRI acquisition sequences implemented on two clinical 1.5 T MR scanner systems: effect of readout bandwidth and echo spacing. *Journal of Applied Clinical Medical Physics*, 11(4):170–180, 2010. ISSN 1526-9914. doi: 10.1120/jacmp.v11i4.3237.

[4] Peter Jezzard and Robert S. Balaban. Correction for geometric distortion in echo planar images from B0 field variations. *Magnetic Resonance in Medicine*, 34(1): 65–73, 1995. ISSN 1522-2594. doi: 10.1002/mrm.1910340111.

[5] Colin Studholme, David John Hawkes, and Derek L. G. Hill. Normalized entropy measure for multimodality image alignment. In *Medical Imaging 1998: Image Processing*, volume 3338, pages 132–143. SPIE, June 1998. doi: 10.1117/12.310835. URL `https://www.spiedigitallibrary.org/conference-proceedings-of-spie/3338/0000/Normalized-entropy-measure-for-multimodality-image-alignment/10.1117/12.310835.full`.

[6] J Mazziotta, A Toga, A Evans, P Fox, J Lancaster, K Zilles, R Woods, T Paus, G Simpson, B Pike, C Holmes, L Collins, P Thompson, D MacDonald, M Iacoboni, T Schormann, K Amunts, N Palomero-Gallagher, S Geyer, L Parsons, K Narr, N Kabani, G Le Goualher, D Boomsma, T Cannon, R Kawashima, and B Mazoyer. A probabilistic atlas and reference system for the human brain: International Consortium for Brain Mapping (ICBM). *Philosophical Transactions of the Royal Society of London. Series B*, 356(1412):1293–1322, August 2001. ISSN 0962-8436. doi: 10.1098/rstb.2001.0915.

[7] Chloe Hutton, Andreas Bork, Oliver Josephs, Ralf Deichmann, John Ashburner, and Robert Turner. Image Distortion Correction in fMRI: A Quantitative Evaluation. *NeuroImage*, 16(1):217–240, May 2002. ISSN 1053-8119. doi: 10.1006/nimg.2001.1054.

[8] Mark Jenkinson. Fast, automated, N-dimensional phase-unwrapping algorithm. *Magnetic Resonance in Medicine*, 49(1):193–197, 2003. ISSN 1522-2594. doi: 10.1002/mrm.10354.

[9] Jesper L. R. Andersson, Stefan Skare, and John Ashburner. How to correct susceptibility distortions in spin-echo echo-planar images: application to diffusion tensor imaging. *NeuroImage*, 20(2):870–888, October 2003. ISSN 1053-8119. doi: 10.1016/S1053-8119(03)00336-7.

[10] Anna van 't Veer. Manual_b0_unwarping_philips_scanner_in_feat_march2017.pdf. March 2017. URL `https://osf.io/hks7x`.

[11] K. Friston and K. Stephan. CHAPTER 3 - Modelling brain responses. In KARL Friston, JOHN Ashburner, STEFAN Kiebel, THOMAS Nichols, and WILLIAM Penny, editors, *Statistical Parametric Mapping*, pages 32–45. Academic Press, London, January 2007. ISBN 978-0-12-372560-8. doi: 10.1016/B978-012372560-8/50003-6.

[12] Martin A. Lindquist and Amanda Mejia. Zen and the Art of Multiple Comparisons. *Biopsychosocial Science and Medicine*, 77(2):114, March 2015. ISSN 2998-8748. doi: 10.1097/PSY.0000000000000148.

[13] Lajos R. Kozák, Louis André van Graan, Umair J. Chaudhary, Ádám György Szabó, and Louis Lemieux. *ICN_Atlas*: Automated description and quantification of functional MRI activation patterns in the framework of intrinsic connectivity networks. *NeuroImage*, 163:319–341, December 2017. ISSN 1053-8119. doi: 10.1016/j.neuroimage.2017.09.014. URL `https://www.sciencedirect.com/science/article/pii/S1053811917307504`.

[14] Rahul S. Desikan, Florent Ségonne, Bruce Fischl, Brian T. Quinn, Bradford C. Dickerson, Deborah Blacker, Randy L. Buckner, Anders M. Dale, R. Paul Maguire, Bradley T. Hyman, Marilyn S. Albert, and Ronald J. Killiany. An automated labeling system for subdividing the human cerebral cortex on MRI scans into gyral based regions of interest. *NeuroImage*, 31(3):968–980, July 2006. ISSN 1053-8119. doi: 10.1016/j.neuroimage.2006.01.021. URL `https://www.sciencedirect.com/science/article/pii/S1053811906000437`.

[15] Matlab R2021a.

[16] SPM 12.

[17] Stephen M. Smith, Mark Jenkinson, Mark W. Woolrich, Christian F. Beckmann, Timothy E. J. Behrens, Heidi Johansen-Berg, Peter R. Bannister, Marilena De Luca, Ivana Drobnjak, David E. Flitney, Rami K. Niazy, James Saunders, John Vickers, Yongyue Zhang, Nicola De Stefano, J. Michael Brady, and Paul M. Matthews. Advances in functional and structural MR image analysis and implementation as FSL. *NeuroImage*, 23 Suppl 1:S208–219, 2004. ISSN 1053-8119. doi: 10.1016/j.neuroimage.2004.07.051.

[18] Lee R. Dice. Measures of the Amount of Ecologic Association Between Species. *Ecology*, 26(3):297–302, 1945. ISSN 0012-9658. doi: 10.2307/1932409. Publisher: [Wiley, Ecological Society of America].

[19] MRIcroGL.

[20] N. Tzourio-Mazoyer, B. Landeau, D. Papathanassiou, F. Crivello, O. Etard, N. Delcroix, B. Mazoyer, and M. Joliot. Automated Anatomical Labeling of Activations in SPM Using a Macroscopic Anatomical Parcellation of the MNI MRI Single-Subject Brain. *NeuroImage*, 15(1):273–289, January 2002. ISSN 1053-8119. doi: 10.1006/nimg.2001.0978.

[21] Sámuel Komoly. *Gyakorlati neurológia és neuroanatómia*. 2018. ISBN 978-963-226-681-7.

Appendix A

Group-level activation maps

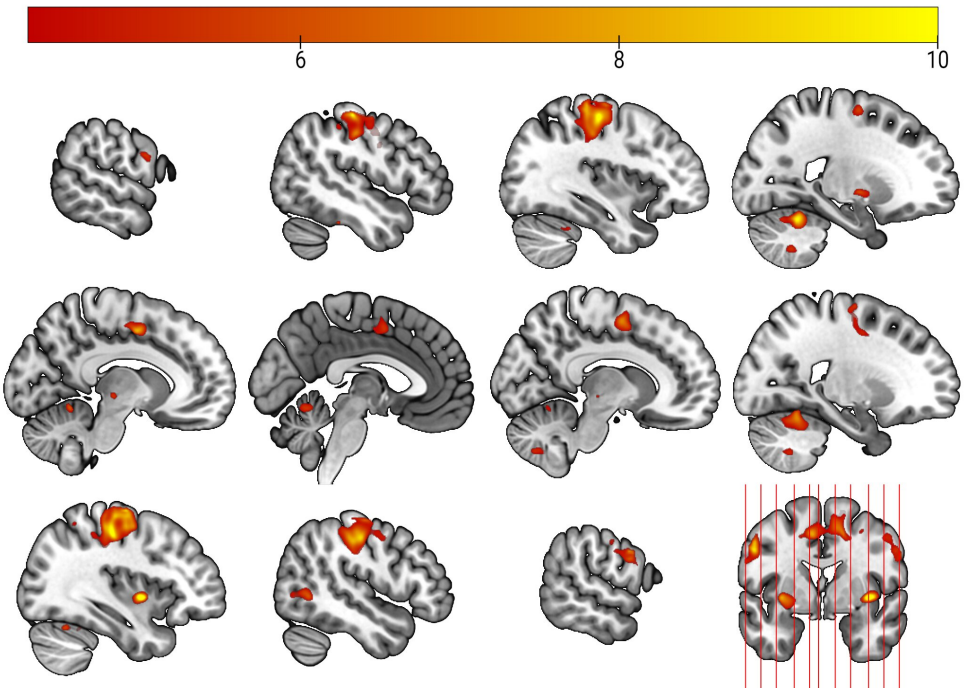

(a)

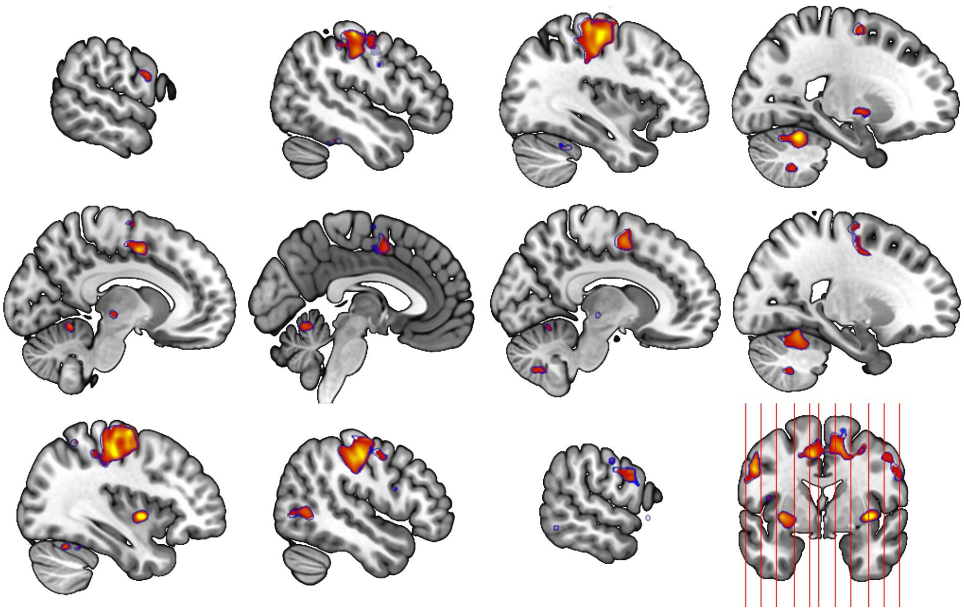

(b)

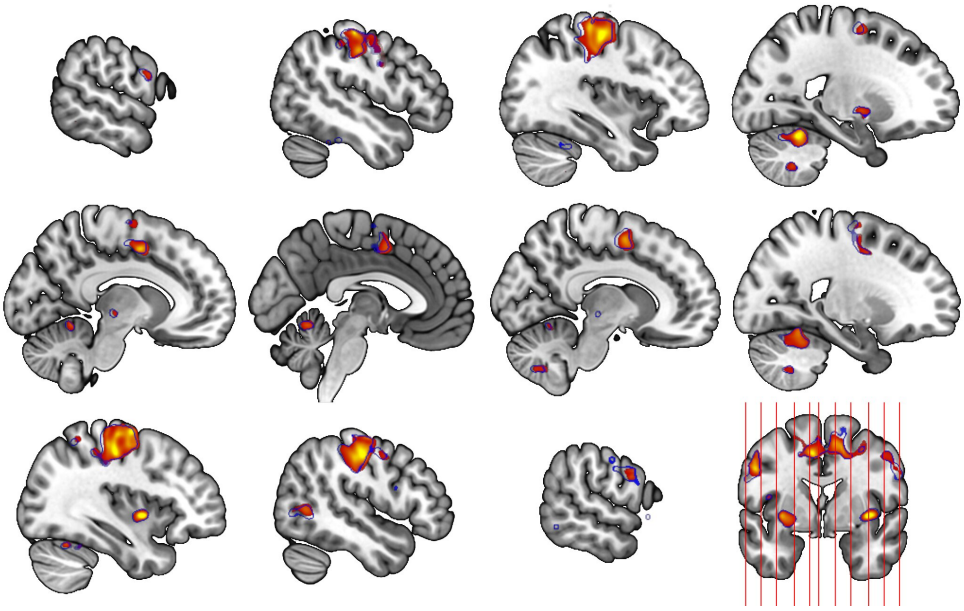

(c)

Figure A.1: Group-level activation maps resulting from the finger tapping task without inhomogeneity correction (a), with dual-echo phase mapping (b) and opposite PE SE-EPI (c) correction. Voxels with $p<0.001$ significance level are highlighted with red to yellow, overlayed on the MNI-152 template. On (b) and (c) the outline of the clusters from the original, not corrected image is overlayed.

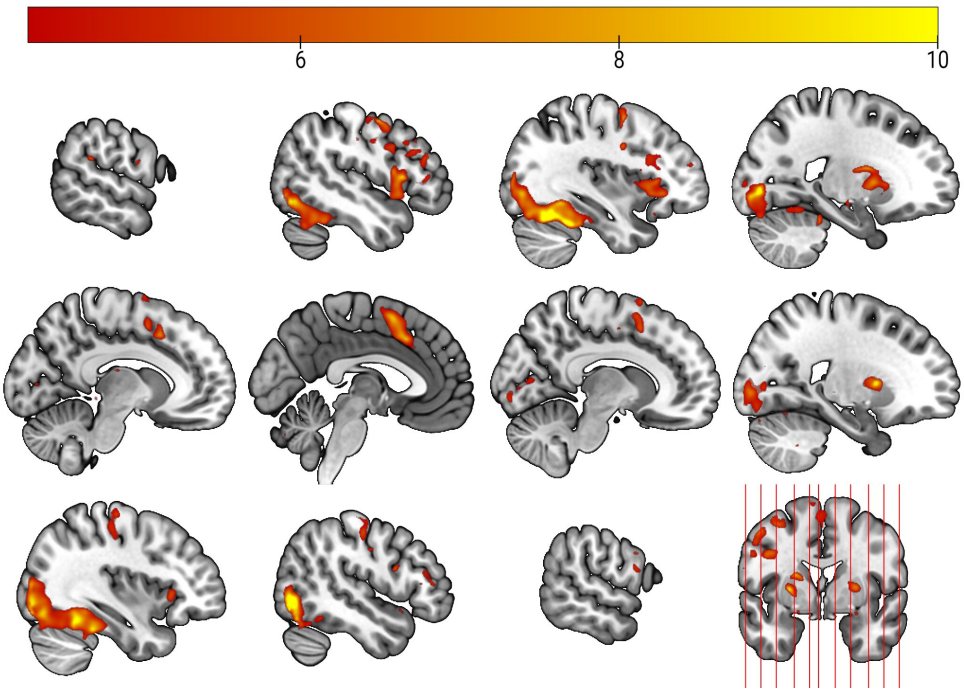

(a)

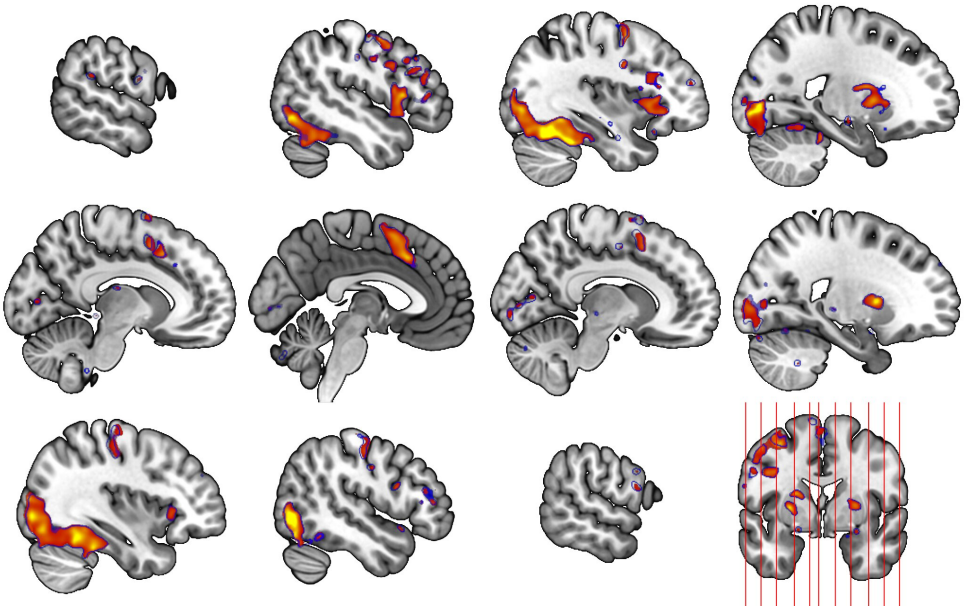

(b)

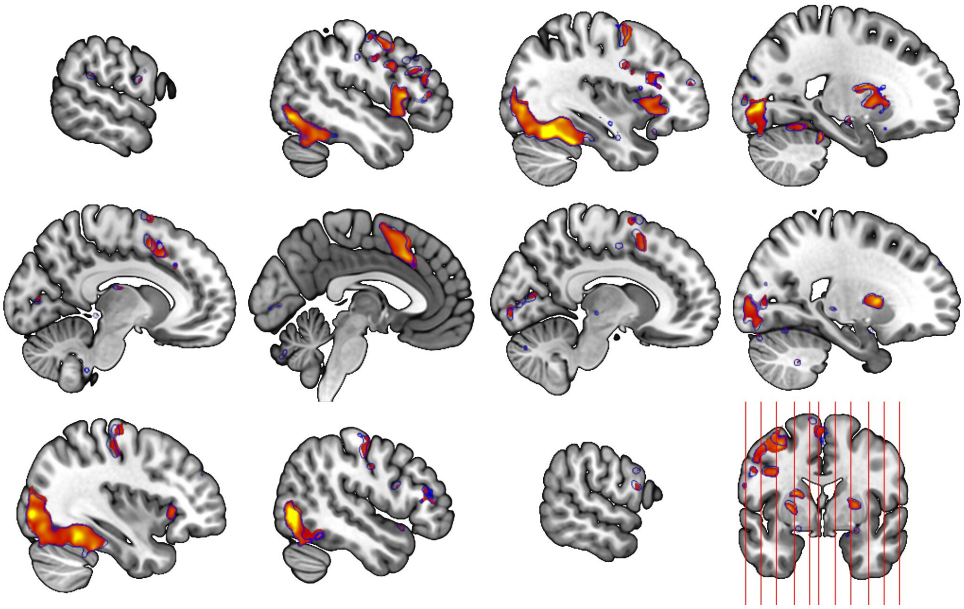

(c)

Figure A.2: Group-level activation maps resulting from the picture naming task without inhomogeneity correction (a), with dual-echo phase mapping (b) and opposite PE SE-EPI (c) correction. Voxels with $p<0.001$ significance level are highlighted with red to yellow, overlayed on the MNI-152 template. On (b) and (c) the outline of the clusters from the original, not corrected image is overlayed.

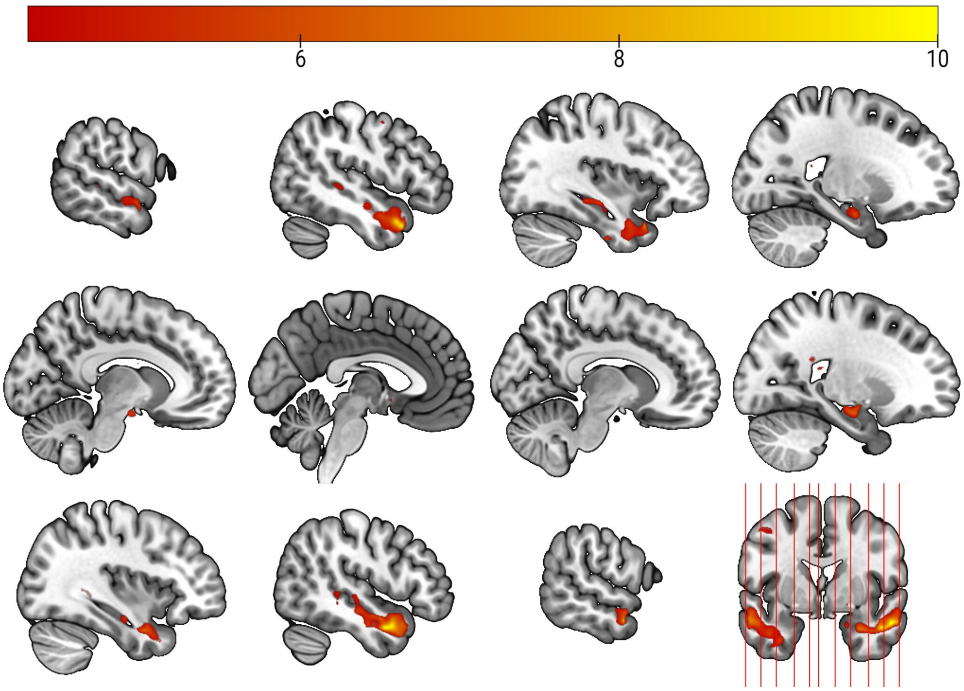

(a)

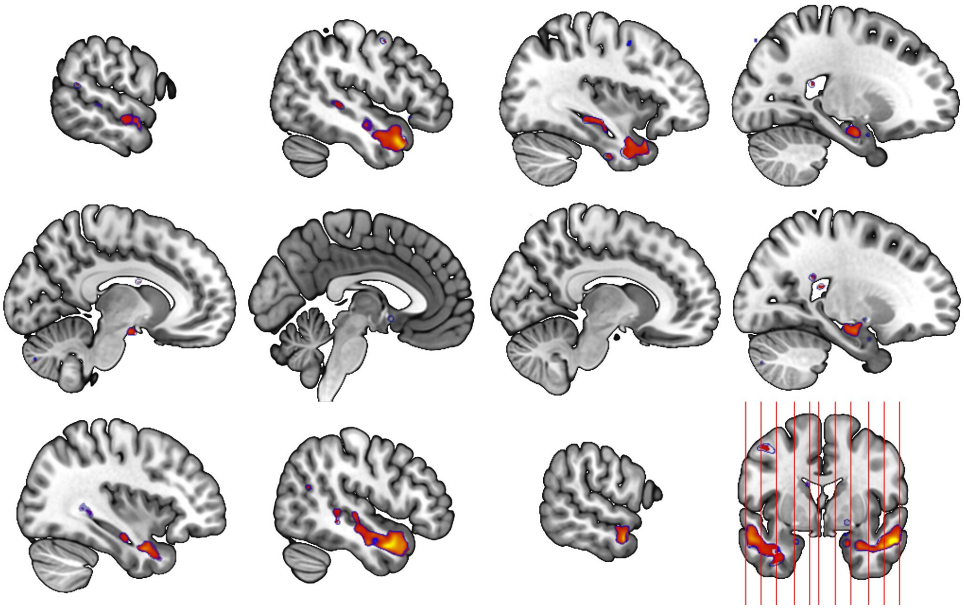

(b)

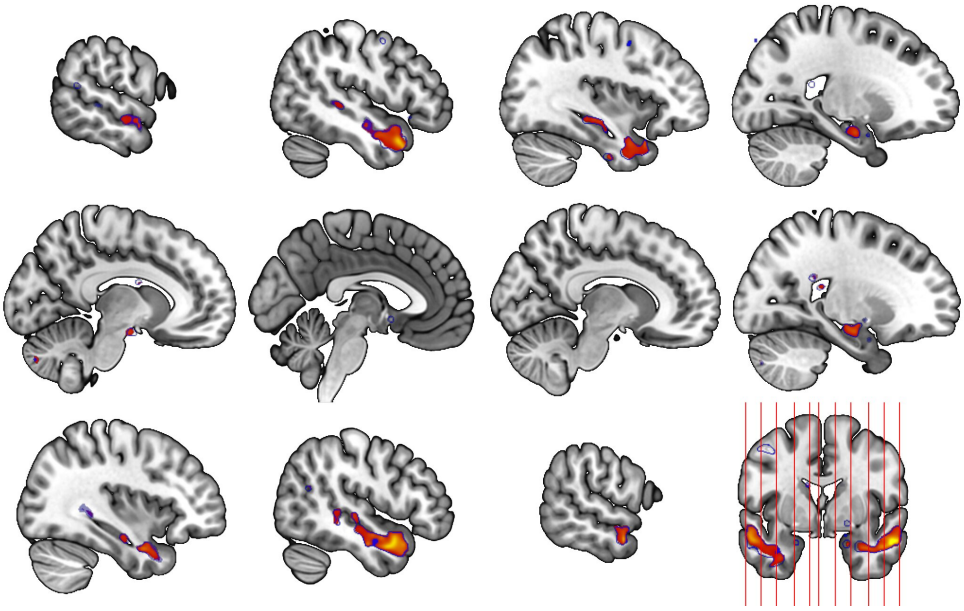

(c)

Figure A.3: Group-level activation maps resulting from the speech comprehension task without inhomogeneity correction (a), with dual-echo phase mapping (b) and opposite PE SE-EPI (c) correction. Voxels with $p<0.001$ significance level are highlighted with red to yellow, overlayed on the MNI-152 template. On (b) and (c) the outline of the clusters from the original, not corrected image is overlayed.